LncRNA GAS5 Suppresses Ovarian Cancer Progression by Targeting miR-96-5p/PTEN Axis

Qian Dong
Shanghai Jiao Tong University School of Medicine Affiliated Renji Hospital
Xiaoran Long
Shanghai Jiao Tong University School of Medicine Affiliated Renji Hospital
Jie Cheng
Shanghai Jiao Tong University School of Medicine Affiliated Renji Hospital
Xia Yin
Shanghai Jiao Tong University School of Medicine Affiliated Renji Hospital
Wenjing Wang
Shanghai Jiao Tong University School of Medicine Affiliated Renji Hospital
Qi Tian
Shanghai Jiao Tong University School of Medicine Affiliated Renji Hospital
Wen Di (diwen163@163.com)
Shanghai Jiao Tong University School of Medicine Affiliated Renji Hospital https://orcid.org/0000-0003-4007-3856

Research

Keywords: lncRNA, GAS5, PTEN, miR-96-5p, ovarian cancer

Posted Date: December 1st, 2020

DOI: https://doi.org/10.21203/rs.3.rs-115366/v1

Abstract

Background

Long non-coding RNAs (lncRNA) play critical roles in tumor occurrence and progression, including ovarian cancer (OC). The lncRNA growth arrest-specific transcript 5 (GAS5) has been proved to be an important modulator in the growth and metastasis of OC cells. Our studies confirm that GAS5 is down-regulated in OC; however, the potential molecular mechanism underlying it remains to be elucidated.

Results

In our study, we demonstrated that the expression levels of GAS5 and PTEN decreased, while miR-96-5p was up-regulated in ovarian cancer samples and cell lines compared with controls. PTEN is the downstream target gene of miR-96-5p. The up-regulation of GAS5 inhibited the expression of miR-96-5p, which directly targets PTEN. GAS5 overexpression can significantly reduce OC cell proliferation and invasion ability via suppression of miR-96-5p expression. PTEN/AKT/mTOR expression had a positive correlation with GAS5 expression. Moreover, miR-96-5p promoted OC progression by mediating PTEN/AKT/mTOR signaling pathway.

Conclusion

Our study identified GAS5 as a ceRNA which regulates the PTEN/AKT/mTOR axis through sponging miR-96-5p in OC.

Background

Ovarian cancer (OC) is one of major malignant tumors of the female reproductive organs with highest mortality rate (1). Ovarian cancer is pathologically classified into several subtypes, including epithelial OC, which accounts for 85–90% of malignant ovarian tumors. Compared with the early stage, the prognosis of pathologically advanced high-grade serous OC is poor, the 5-year overall survival rate of which is only 27% (2). Despite current therapies, efficient treatment designed to prevent recurrence remains limited. Therefore, an in-depth understanding of the underlaying mechanism of OC will contribute to the development of novel and effective therapy strategies.

Long non-coding RNA (lncRNA) is a subclass of endogenous, non-protein coding RNA, which lacks an open reading frame and usually consists of more than 200 nucleotides(3). increasing evidence suggested that lncRNAs are involved in various biological processes such as gene transcription, genomic imprinting, transcriptional activation, epigenetic modification, and miRNA regulation (4). Undoubtedly, lncRNAs have been investigated of their role in the cancer development. LncRNAs have emerged as new potential cancer treatment strategy (5). Growth arrest-specific transcript 5 (GAS5), an important lncRNA, is transcribed from the non-protein encoded small nucleolar RNA (snoRNA) gene GAS5 (6). Altered GAS5 have been demonstrated in many different cancers. In cervical cancer, studies have revealed that GAS5

can regulate resistance to cisplatin by regulating miR-21 (7). In prostate carcinoma, lncRNA GAS5 can target miR-103 through the AKT/mTOR signaling pathway and inhibits proliferation and progression of prostate cancer (8). In colorectal cancer, GAS5 snoRNAs were associated with p53 expression and has a close relation with DNA damage level (9). A previous study confirmed that the level of lncRNA GAS5 reduced in OC with great significance and indicated a poor prognosis (10). However, the biological mechanism of GAS5 in the ovarian cancer is largely unknown.

MicroRNAs (miRNA) are a group of, non-coding RNAs that consist of nearly 22 nucleotide and can negatively regulate gene expression in a post-transcriptional manner (11, 12). MiRNAs play an essential part in various biological processes, like cell proliferation, autophagy, apoptosis and differentiation (13). At the same time miRNAs demonstrated critical roles in OC in prior studies (14). Recently, researches revealed the vital role of miR-96-5p in tumor development. For example, miR-96-5p influences radio-sensitivity of HNSCC cell lines by targeting phosphatase and tension homolog deleted on chromosome ten (PTEN) expression (15). miR-96 can also improve human cancer cellular sensitivity to cisplatin and PARP inhibition (16). In pancreatic cancer, miR-96-5p can inhibit KRAS function, acting as a tumor suppressor.

In this study, we showed that the expression of lncRNA GAS5 was low among advanced OC patients. As far as we can see, this study initially confirmed that lncRNA GAS5 overexpression can inhibit cell proliferation and invasion via mediating the miR-96-5p/PTEN-signaling axis in OC patients. As a result, this study can be used as a reference version for clinical treatment of ovarian cancer by investigating the possible function of lncRNA GAS5 through miR-96a-5p/PTEN axis.

Results

Overexpression of GAS5 suppressed the proliferation of OC cells in vivo

We previously confirmed the GAS5 down-regulation in ovarian cancer tissues. Microarray results (3 EOC samples vs. 3 normal samples) demonstrated that lncRNA GAS5 expression level was significantly lower in cancer samples. Real-time qPCR also revealed that GAS5 had a significantly lower expression in 53 EOC samples, when compared to ten normal ovarian samples. Similarly, in cell lines, the expression of GAS5 was obviously reduced when comparing OC cell lines with normal human ovarian epithelial cell line. Conversely, GAS5 expression was positively associated with International Federation of Gynecology and Obstetrics(FIGO) stage and histological type (Data not shown)(17). The present results are consistent with the Gene Expression Profiling Interactive Analysis (GEPIA) database. Herein, GAS5 was down-regulated in most tumors, including OC (Fig. 1A). Following transfection with GAS5 expression vector, real-time qPCR exhibited overexpression of GAS5 in SKOV3 and HEY cell lines (Fig. 1B and C). Figure 1D revealed GAS5 overexpression in cells transfected with GAS5 expression vector rather than in those transfected with empty vector ($P < 0.01$, Fig. 1D). Moreover, in a mouse xenograft model, we investigated the growth inhibition/anti-tumor effects of GAS5 in vivo. The mice were randomly distributed into control group (NC group) and GAS5 stable overexpression group (GAS5 group). After five weeks, as

shown in Fig. 1F, G and H, the tumor number and tumor weight were significantly decreased by GAS5 injection. Nevertheless, there was no difference in weight between these two groups (Fig. 1E). Furthermore, we compared PTEN expression in the tumor tissues of nude mouse by immunohistochemical staining. The results showed that the proportion of positive cells in the GAS5 overexpression group were lower than that of the NC group in Fig. 2A ($P < 0.05$).

GAS5 suppressed proliferation and migration ability of OC cells in vitro

CCK-8 assay and colony formation assay revealed that GAS5 overexpression significantly reduced the proliferation of OC cells *in vitro* ($P < 0.01$) as shown in Fig. 2B. Viability of HEY and SKOV3 cell lines were assessed after LV-GAS5 transduction($P < 0.05$) as shown in Fig. 2C, the wound-healing assay showed that overexpression of GAS5 can decrease the cell migratory capacity both in HEY and SKOV3 cells (Fig. 3A and B). The results of transwell assay suggested that GAS5 overexpression decreased migration ability of OC cells *in vitro* (Fig. 3C and 3D).

lncRNA GAS5 influences PTEN expression by competitive binding with miR-96-5p

To explore the potential molecular mechanism of GAS5 in OC progression, we first investigated the related recruitment of miRNAs. Microarray results (3 EOC samples vs. 3 normal samples) demonstrated that lncRNA GAS5 expression was remarkably decreased in cancer samples in our previous research, at the same time ,miRNAs were involved in the occurrence of OC cells as shown in our results of Agilent ceRNA in heatmaps showing top 9 miRNAs (Fig. 4C). Bioinformatic analysis indicates that GAS5 possesses the conserved target site of miR-96-5p with a high affinity score (http://carolina.imis.athenainnovation.gr/diana_tools/web/index.php?r=site/tools). Fluorescence in situ hybridization (FISH) images indicated that lncRNA GAS5 was located in the cytoplasm and the nucleus of the SKOV3 (Fig. 4E). Furthermore, real-time qPCR showed the expression level of miR-96-5p in the empty vector group and GAS5 group. We found that the expression of miR-96-5p was significantly lower in GAS5 overexpression cell lines compared with that in the normal OC cell line ($P < 0.05$) (Fig. 4D). Subsequently, Dual-Luciferase Reporter Gene Assay was applied to confirm the relationship among lncRNA GAS5 and miR-96-5p. Compared with the empty vector group, luciferase activity of the GAS5 WT-binding site was inhibited by miR-96-5p ($P < 0.001$), while the GAS5 MUT-binding site was not affected ($P > 0.05$). MiR-96-5p could specifically bind to lncRNA GAS5 (Fig. 4A). These data indicated that GAS5 functioned as a ceRNA of miR-96-5p. Moreover, we performed RIP assay based on Ago2. We overexpressed lncRNA GAS5 in SKOV3 cells then pulled down Ago2 using anti-Ago2 antibody. Overexpression of GAS5 can result in a significant decrease in the enrichment of PTEN transcripts pulled down by Ago2 ($P < 0.01$) in Fig. 4B, indicating that there existed miRNA-bound PTEN transcripts. lncRNA GAS5 can compete with the PTEN transcript for the binding of miRNAs.

GAS5 and miR-96-5p regulate proliferation and migration of OC cells

To determine whether miR-96-5p or lncRNA GAS5 influences OC cell proliferation and migration, miR-96-5p mimics were generated. qPCR results showed that expression of miR-96-5p was enhanced under the influence of miR-96-5p mimic ($P < 0.001$) (Fig. 4F). CCK-8 assay was performed to analyze the effects exerted by GAS5 and miR-96-5p on OC cells proliferation. GAS5 up-regulation and miR-96-5p down-regulation deterred the proliferation of OC cells compared with the NC group ($P < 0.05$) (Fig. 5A, 5B). The scratch test revealed that compared to the control group in HEY cell lines, cellular migration ability was enhanced in miR-96-5p mimic groups($P < 0.01$), while miR-96-5p inhibitor groups were declined （$P < 0.01$), It was drawn that down-regulated GAS5 expression and up- regulated miR-96-5P expression induced strong migration ability of ovarian cancer cells than NC group($P < 0.001$).Furthermore, up-regulated GAS5 expression and down- regulated miR-96-5P expression retrained migration ability than NC group ($P < 0.001$) as shown in Fig. 5C. Similar results were obtained from the SKOV3 cell line (Fig. 5D). Colony formation assay was applied to analyze the effects exerted by GAS5 and miR-96-5p on proliferation of OC cells. GAS5 up-regulation and miR-96-5p down-regulation deterred the proliferation of OC cells compared with the NC group ($P < 0.01$; $P < 0.001$) (Fig. 6A and B).

lncRNA GAS5 and miR-96-5p repress invasion ability of OC cells

By transwell assay, we observed the influence of OC cell invasion by miR-96-5p or lncRNA GAS5. As shown in Fig. 7A-D, the invasion ability of HEY cells in the control group was not significant influenced ($P > 0.05$), while in the oe-lncRNA GAS5 and miR-96-5p inhibitor groups, the invasion ability was inhibited ($P < 0.05$). Compared with oe-lncRNA GAS5 and miR-96-5p inhibitor groups, the invasion ability increased in oe-lncRNA GAS5 + miR-96-5p mimic and miR-96-5p mimic groups (all $P < 0.05$). Similar results were observed in the SKOV3 cell line (Fig. 7A-D).

lncRNA GAS5 promotes OC cell apoptosis through interaction with miRNA-96-5p

Apoptosis of SKOV3 cells was detected by flow cytometry after transfection of GAS5 and miR-96-5p for 72 h. As shown in Fig. 8A, compared with control group, the apoptosis rate of oe-lncRNA GAS5 group ($P < 0.05$) and miR-96-5p inhibitor group ($P < 0.05$) increased significantly in SKOV3 cells, but it decreased in the miR-96-5p mimic and oe-lncRNA GAS5 + miR-96-5p mimic groups ($P < 0.05$). Similar trends were found in the HEY cell line (Fig. 8B).

Upregulation of lncRNA GAS5 increases PTEN protein level but inhibits phosphorylation of AKT

As the PTEN/AKT/mTOR pathway is essential for cell proliferation and invasion, we investigated the correlations of GAS5, miR-96-5p and the PTEN/AKT/mTOR pathway in OC cells. Bioinformatic analysis showed that there were specific binding sites between the sequences of miR-96-5p and 3′ UTR of PTEN and between GAS5 and sequences of miR-96-5p. We also found that the luciferase activity of the PTEN-3′ UTR (WT) was significantly inhibited by miR-96-5p ($P < 0.05$), whereas the activity of PTEN-3′ UTR (MUT) was not affected ($P > 0.05$), indicating that miR-96-5p specifically bound to PTEN-3′ UTR and reduced the expression of PTEN after transcription (Fig. 9A and B). Western blot examined the protein expression of the PTEN pathway in the HEY and SKOV3 cell lines. Compared with the control group, protein expression of PTEN did not show significant differences in the empty vector group (all $P > 0.05$). In contrast to the control group, the oe-lncRNA GAS5 group and miR-96-5p inhibitor group revealed increased protein expression of PTEN, but decreased phosphorylation of AKT, N-cadherin, Snail, PI3K-p85, and P-mTOR (all $P < 0.05$). Protein expression of PTEN was lower, while phosphorylation of AKT, N-cadherin, Snail, PI3K-p85, and mTOR was higher in the oe-lncRNA GAS5 + miR-96-5p mimic group than those in the oe-lncRNA GAS5 and miR-96-5p inhibitor groups (all $P < 0.05$). However, protein expression of PTEN did not differ significantly between the oe-lncRNA GAS5 and miR-96-5p inhibitor groups (all $P > 0.05$). The protein expression of AKT remained nearly the same among all groups in the HEY cell line (Fig. 9C). Further, the results were similar in the SKOV3 cell line (Fig. 9D).

Discussion

More and more studies have confirmed the important role of lncRNAs in numerous biological processes. Aberrantly expressed lncRNAs has been discovered and investigated in the pathogenesis and development of OC. This study shows that lncRNA GAS5 can inhibit OC cell proliferation and promote apoptosis by negatively targeting miR-96-5p/PTEN axis.

GAS5 expression has been examined in various cancers including breast, ovarian, and cervical carcinomas (17–20). We previously confirmed that GAS5 expression in human tumor cells is relatively lower than that of the normal tissues (21), in agreement with the speculation that GAS5 exerts an anti-proliferative, tumor-suppressing function. lncRNA GAS5 is involved in cell proliferation, drug resistance, tumor cell invasion, apoptosis, and autophagy. However, the detailed underlying mechanism remains unclear. Our study concentrated on the biological role of lncRNA GAS5 in OC.

We observed that upon GAS5 overexpression, OC cell proliferation was suppressed and apoptosis increased, concurrent with the function of GAS5 in other carcinomas, including pancreatic cancer and breast cancer (22, 23). ceRNA, including lncRNA, binds to miRNA and serves as a “sponge” to absorb miRNA in cells. It is well-known that miRNA can bind to the 3′ UTRs of the mRNAs of target gene, thus regulating their expression. As an effective miRNA sponge, lncRNAs are primarily located in the cytoplasm (24, 25). We isolated RNA from the nucleus and cytoplasm of SKOV3 cells. The FISH assay revealed lncRNA GAS5 upregulation in the cytoplasm, suggesting that lncRNA GAS5 can play a regulatory role in a ceRNA-dependent manner. Therefore, we speculated that GAS5 can bind to miRNAs to exert its function, concurrent with previous reports. For example, GAS5 positively regulates miR-222 in colorectal

cancers (26). Other lncRNA, including PTAR, also binds to miR-101-3p to regulate zinc finger E-box-binding homeobox 1 (ZEB1) expression, promoting epithelial–mesenchymal transition (EMT) and invasion in OC (27). We investigated the related recruitment of miRNAs. Microarray results (3 EOC samples vs. 3 normal samples) demonstrated that top 9 miRNAs were involved in the occurrence of OC cells as shown in our results of Agilent ceRNA in heatmaps. Bioinformatics analysis indicates that GAS5 possesses the conserved target site of miR-96-5p with a high affinity score. The overexpression of miR-96-5P has been discovered in HNSCC (15), and LncRNA GAS5 acts as a competing endogenous RNA of miR-96-5p in renal tubular epithelial fibrosis (28). The results of luciferase reporter assay confirmed the interaction between lncRNA GAS5 and miR-96-5p. The results showed that the binding of lncRNA GAS5 to miR-96-5p was sequence-specific. miRNA regulates stability and translation of mRNA at the post-transcriptional level (29). It suggests that GAS5 exerts its biological functions by directly binding with miR-96-5p.

PTEN is a tumor-suppressor gene that is frequently deleted or mutated in various human cancers (30). PTEN can be regulated by PI3K/AKT. Up-regulation of PTEN can reduce the generation of reactive oxygen species in cells (31). Furthermore, PTEN might be a potential target of miR-96-5p as predicted by bioinformatic method. PTEN influences OC progression (32, 33). Increasing evidence indicates that miRNA is vital during the pathogenesis of tumors and can affect invasion and proliferation of tumors by regulating the PI3K/AKT signing pathway(34). For example, lamin A/C protein can promote prostate cancer cell growth, migration, and invasion through the PI3K/AKT/mTOR pathway (35). Moreover, the PI3K/AKT/mTOR pathway contributes to neuroprotection in a traumatic brain injury through PPAR(36). Inactivation of PTEN is positively correlated with the aggressive capacity of OC, whereas PTEN plays a tumor-suppressive role in OC (37, 38). Our study initially identified an inverse relationship between miR-96-5p and PTEN expression levels in ovarian cell lines through bioinformatics analysis (http://zmf.umm.uni-heidelberg.de/apps/zmf/mirwalk2/). Dual-luciferase reporter assay also confirmed the interaction between miR-96-5p and PTEN. Therefore, we can infer that miR-96-5p is at least partially responsible for oncogenic role of PTEN. Moreover, miR-96-5p inhibited proliferation proteins by targeting PTEN. The relationship between lncRNA GAS5 and PTEN was further testified by western blot assay. The rescuing experiment results showed that lncRNA GAS5 upregulated PTEN expression and suppressed expression of cell proliferation and migration-related proteins by acting as a miR-96-5p sponge. Mice models overexpressing lncRNA GAS5 were established by intraperitoneal injection of transfected GAS5 OC. We found that overexpression of lncRNA GAS5 significantly inhibited tumor metastasis and growth, and PTEN expression in tumor tissues. It has been reported that GAS5 inhibits the proliferation, migration, invasion, and epithelial stromal transformation of OSCC by regulating miR21/PTEN axis (39). In the present study, the activation of PTEN/AKT/mTOR was enhanced when GAS5 was overexpressed. These results demonstrate that GAS5 can regulate PTEN/AKT/mTOR pathway in OC.

Although we demonstrated the role of the AKT/PTEN signaling pathway in OC cells, the mechanism underlying the activation of the AKT/PTEN pathway by LncRNA GAS5 and miR-96-5p has not been completely elucidated; therefore, it warrants further investigations.

Conclusion

lncRNA GAS5 as a ceRNA which regulates the PTEN/AKT/mTOR axis through sponging miR-96-5p in OC. lncRNA GAS5 overexpression can inhibit cell proliferation and invasion via mediating the miR-96-5p/PTEN-signaling axis in OC patients. this study can be used as a reference version for clinical treatment of ovarian cancer by investigating the possible function of lncRNA GAS5 through miR-96a-5p/PTEN axis.

Methods

Microarray analysis

Total RNA in the ovarian tissue RNA samples were hybridized to SBC Human (4 × 180 K) ceRNA microarray (Shanghai Biotechnology Co, Shanghai, China). Quantile normalization was applied using GeneSpring GX v11.5.1 software (Agilent Technologies). lncRNAs with differential expression were selected according to the criteria of change fold ≥ 2 and $P < 0.05$ as previously described (17) .

Cell culture

Human OC cell lines HEY and SKOV3 were obtained from China Academia of Sciences (Shanghai, China). Cells were cultured in Dulbecco's modified Eagle medium (Gibco, USA) with 10% fetal bovine serum (HyClone, USA). All cells were cultured at 37 °C with 5% CO_2 in a humidified atmosphere. When the cells adhered to the wall bottom, they were digested by 0.25% trypsin for subculture. Cells at the logarithmic growth phase were collected for further experiments.

Cell transfection

Human GAS5 gene (NR_002578) with the BamHI and XhoI restriction site sequences was synthesized (GenePharma, Shanghai, China). After achieving retrovirus-mediated stable expression of GAS5 in SKOV3 and HEY cell lines, real-time quantitative polymerase chain reaction (real-time qPCR) was conducted to validate GAS5 overexpression in the two cell lines (Fig. 1D) and a mimic-miR-96-5p (sense, 5′-UUUGGCACUAGCACAUUUUUGCU-3′; antisense, 5′-CAAAAAUGUGCUAGUGCCAAAUU-3′) was synthesized. The empty vector pcDNA3.1 and scramble siRNA were used as control. Lipofectamine 2000 reagent (ThermoFisher) was utilized for transfection. After 24 h, cells were harvested for subsequent experiments. Real-time qPCR was used to assess transfection efficacy.

Cell Counting Kit-8 Assay

Cell proliferation was tested using Cell Counting Kit-8 (CCK-8) assay (Dojindo Molecular Technologies, Kumamoto, Japan). Briefly, OC cells were plated with 5×10^3 cells per well in 96-well plates. At specific time points (12, 24, 48, and 72 h), the original supernatants were removed from each well and 100 μL culture medium with 10 μL CCK-8 solution was added ,after which cells were incubated at 37 °C for 2 h. Cell viability was evaluated by a microplate reader (Multiskan MK3, Thermo Scientific, USA).

Colony formation assay

A total of 1×10^3 HEY and SKOV3 cells were plated in 6-well plates to disperse the cells evenly. Following incubation at 37 °C in 5% CO_2 for 10–14 days, the culture was terminated when the colonies were visible by eye. The original medium was removed, and the cells were washed twice by phosphate-buffered saline (PBS). Subsequently, the colonies were fixed by methanol at − 20 °C for 15 min and stained with crystal violet for 20 min. Then the staining fluids were rinsed off. Images were taken from the stained plates under low magnification, and segments labeled on the plates were identified as scale. The colonies with a diameter larger than scale size were included for calculation.

Wound-healing assay

Cell migration ability was assessed by wound-healing assay. Briefly, 2×10^5 SKOV3 and HEY cells were cultured in 6-well plates. After 24 h, a thin wound was made by scraping with a sterile pipette tip across the center of each well. The cells were then cultured for 24 and 48 h for the observation of the wound. Five random views of each well were captured under microscope.

Transwell Assay

In total, 2×10^5 cells were transfected after 48 h and resuspended in serum-free DMEM. Two-hundred-milliliter cell suspensions were placed in the upper chambers with an 8 μm pore size polycarbonate membrane Transwell insert (Corning Costar, MD, USA) coated with 50 μL of Matrigel (1:4 dilution in a serum-free medium), and 600 mL DMEM supplemented with 10% serum as a chemotactic factor was added in the lower chambers, following a 24 h incubation, cells were stained with crystal violet for those across the porous membrane.

Flow cytometry

HEY and SKOV3 cells were cultured in a 6-well plate with 5×10^6 per well at 37 °C and were classified into oe-GAS5 or NC groups. Cells were then digested by 0.25% trypsin without EDTA and resuspended in 100 μL of 1 × binding buffer at a density of 1×10^6 /mL staining with Annexin V-fluorescein isothiocyanate (FITC)/propidium iodide (PI). Fluorescence intensity was detected by FACScan flow cytometer (BD Biosciences) to determine the percentage of apoptotic cells.

Dual-luciferase reporter gene assay

Bioinformatics prediction websites were used for the possible binding sites of miR-96-5p and lncRNA GAS5. Several prediction target tools, such as miRWalk3 (http://zmf.umm.uni-heidelberg.de/apps/zmf/mirwalk2/) and DIANA Tools (http://carolina.imis.athenainnovation.gr/diana_tools/web/index.php?r=site/tools), were used. The full length of GAS5 and the 3′ UTR of PTEN were amplified separately and cloned into a pmirGLO Dual-Luciferase miRNA Target Expression Vector (Promega, USA). pGAS5-MUT (mutant type) and pPTEN-MUT vectors were constructed using the pRL-TK vector (Promega, USA). MiR-96-5p mimic and miR-96-5p

empty vectors were separately co-transfected with luciferase reporter gene vector into HEY and SKOV3 cells. Luciferase activity was detected using the kit (Promega, USA).

Real-time qPCR

TRIzol reagent (Invitrogen, Thermo Fisher Scientific, USA) and the Universal microRNA Purification Kit (EZBioscience, USA) was used to extract total RNA according to protocol. Then, cDNAs were synthesized using PrimeScript RT-PCR kit (TakaraBio, Japan). PCR was conducted on an ABI 7500 Real-Time PCR System (Applied Biosystems, Foster City, USA) using SYBR Premix Ex Taq II kit (Takarabio, Japan) with a miRNA-specific 5′ primer (has-miR-96-5p: CGGTTTGGCACTAGCACATTTTTG). The primer sequences for GAS5 were as follows: forward, 5′-GGTATGGAGAGTCGGCTTGA-3′ and reverse, 5′-GCAAGACCCTTTCAAGCAGT-3′. GAPDH was used as an internal control for mRNAs with primers as follows: forward, 5′-GAAGGTGAAGGTCGGAGTC-3′ and reverse, 5′-GAAGATGGTGATGGGATTTC-3′. U6 forward, 5′-CTCGCTTCGG CAGCACA-3′, and reverse, 5′-AACGCTTCACGAATTTGCGT-3′ was used as an internal control for miRNAs. Gene expression was analyzed using the ΔΔCq method.

RNA immunoprecipitation assays

SKOV3 cells were transfected with LV-GAS5 and LV-NC. RNA immunoprecipitation assay (RIP) was carried out according to the protocols. The RIP buffer contained magnetic beads conjugated with IgG (control) and the Ago2 antibody (Abcam, ab32381, UK), and was used to obtain the cell lysate. Magna RIP RNA-Binding Protein Immunoprecipitation Kit (EMD Millipore, USA) was applied for RNA immunoprecipitation. RNAs were then isolated and quantified by Qubit 3.0 (Life Technologies, US). The co-precipitated RNAs were detected by qPCR and were performed to examine the expression levels of lncRNA GAS5 and PTEN.

Western blot

Total protein was extracted and separated using 10% SDS-PAGE (sodium dodecyl sulfate -polyacrylamide gel electrophoresis) and transferred to polyvinylidene fluoride (PVDF) membranes (Millipore, USA). Subsequently, the membranes were then blocked in 5% skimmed milk, and incubated with primary antibodies at 4 °C overnight. After blocking with 5% BSA (Sigma-Aldrich; USA) at 37 °C for 1 h, the membrane was incubated with primary antibodies of PTEN (1:1,000; cat. no. 9188T; Cell Signaling Technology, USA), AKT (1:1,000; cat. no. 4691T; Cell Signaling Technology, USA), p-AKT (1:2,000; cat. no. 4060T; Cell Signaling Technology, USA), N-Cadherin (1:1,000; cat. no. 13116T; Cell Signaling Technology, USA), PI3K-p85 (1:1,000; cat. no. 173665; Cell Signaling Technology, USA), Cleaved Caspase-3 (1:1,000; cat. no. 9664T; Cell Signaling Technology, USA), Snail (1:1,000; cat. no. 3897T; Cell Signaling Technology; USA), p-mTOR (1:1,000; cat. no. 5536T; Cell Signaling Technology, USA) and β-actin (1:500; cat. no. F3002; Sigma-Aldrich, USA) at 4 °C overnight. Following incubation with a horseradish peroxidase (HRP)-conjugated goat anti-rabbit (1:5,000; cat. no. ab205718; Abcam) or goat anti-mouse (1:5,000; cat. no. ab205719; Abcam) secondary antibody at 4 °C for 2 h, densitometric analysis was performed using ImageJ v2.4.1 (National Institutes of Health) with protein expression levels normalized to β-actin.

Tumorigenicity assays in nude mice

Animal studies were approved by the committee for the use and care of animals of Renji Hospital (Shanghai, China) with the approval number (39) 114. Briefly, HEY cells were stably transfected with different vectors (Lenti-GAS5 overexpression or Lenti-control) for 72 h. The cells were then harvested for the injection. Four to six weeks old nude mice were randomly divided into two groups: NC group and GAS5 group (n = 6 in each group) and injected subcutaneously approximately 6×10^6 cells diluted in 200μL PBS from right flanks. Tumors were evaluated every week for 5 weeks. The observation was stopped and the mice were executed in 35 days. Tumor development was monitored, The difference in the number of visible tumors and the weight between the two group and tumor sizes were measured. The tumor volume (V) was calculated from the formula: $V = ½ (\text{length} \times \text{width}^2)$. The protein expression levels in tumors of the two groups were also detected though immunohistochemistry.

Immunohistochemistry

The sections were prepared after tissues from nude mice were embedded in paraffin. Expression of PTEN were detected by staining. Slides were observed under the microscope (400⊆) (Olympus, Japan). The results were graded by the percentage of positive cells.

RNA-fish

Cy3-labeled GAS5 and DAPI-labeled U6 probes were customized from RiboBio (Guangzhou, China). RNA FISH were conducted according to fluorescent in situ hybridization kit by following manufacturer's instructions.

Statistical analysis

Statistical analysis was performed by the software SPSS 22.0. Quantitative results were expressed as mean ± standard deviation (SD) and were compared using Student's *t*-test. P values less than 0.05 were considered statistically significant.

Abbreviations

ANOVA Analysis of variance

FISH Fluorescence in situ hybridization

GEPIA Gene Expression Profiling Interactive Analysis

OC Ovarian cancer

PBS Phosphate-buffered saline

PI Propidium iodide

RIPA RNA immunoprecipitation assay

SD Standard deviation

lncRNA Long non-coding RNAs

GAS5 growth arrest-specific transcript 5

ceRNA competing endogenous RNA

PTEN phosphatase and tensin homolog deleted on chromosome ten

Declarations

Ethics approval and consent to participate

This study was conducted in accordance with the Declaration of Helsinki principles. It was approved by the Medical Research Ethics Committee of Renji Hospital, School of Medicine, Shanghai Jiao Tong University.

Availability of data and materials

The analyzed data sets generated during the study are available from the corresponding author on reasonable request.

Acknowledgments

We thank all support from Department of Obstetrics and Gynecology, Ren Ji Hospital, School of Medicine, Shanghai Jiao Tong University. The authors are grateful to all staff members who contributed to this study.

Funding

This work supported by the National Key Research and Development Program (863) of China (No. 2016YFC1302900), the National Natural Science Foundation of China (No. 81772770), the Science and Technology Commission of Shanghai Municipality (No. 18441904800), the Shanghai Municipal Commission of Health and Family Planning (No. 2017ZZ02016 and ZY(2018-2020)-FWTX-3006), the Shanghai Municipal Key Clinical Specialty and the Program of Shanghai Hospital Development Center (16CR2001A).

Availability of data and materials

All data generated or analysed during this study are included in this published article.

Author Contributions

QD and XRL designed and performed the experiments, analyzed the data, and wrote the manuscript. JC helped analyze the experimental data and write the manuscript. QT and WJW helped analyze the data. XY provided tissue samples. WD conceptualized and designed the study and critically revised the manuscript. All authors read and approved the final version of the manuscript.

Consent for publication

Not applicable.

Competing interests

The authors declare that they have no competing interests.

References

1. Jayson GC, Kohn EC, Kitchener HC, Ledermann JA. Ovarian cancer. Lancet. 2014;384(9951):1376–88.
2. Torre LA, Trabert B, DeSantis CE, Miller KD, Samimi G, Runowicz CD, et al. Ovarian cancer statistics, 2018. Cancer J Clin. 2018;68(4):284–96.
3. Alessandro F, Irene B. Long non-coding RNAs: new players in cell differentiation and development. Nat Rev Genet. 2014;15(1):7–21.
4. Mercer TR, Dinger ME, Mattick JS. Long non-coding RNAs: insights into functions. Nat Rev Genet. 2009;10(3):155–9.
5. Chen G, Wang Z, Wang D, Qiu C, Liu M, Chen X, et al. LncRNADisease: a database for long-non-coding RNA-associated diseases. Nucleic Acids Res. 2013;41(Database issue):D983-D6.
6. Smith CM, Steitz JA. Classification of gas5 as a Multi-Small-Nucleolar-RNA (snoRNA) Host Gene and a Member of the 5'-Terminal Oligopyrimidine Gene Family Reveals Common Features of snoRNA Host Genes. Molecular Cellular Biology. 1998;18(12):6897–909.
7. Wen Q, Liu Y, Lyu H, Xu X, Wu Q, Liu N, et al. Long Noncoding RNA GAS5, Which Acts as a Tumor Suppressor via microRNA 21, Regulates Cisplatin Resistance Expression in Cervical Cancer. International Journal of Gynecological Cancer Official Journal of the International Gynecological Cancer Society. 2017;27(6):1096.
8. Xue D, Zhou C, Lu H, Xu R, Xu X, He X. LncRNA GAS5 inhibits proliferation and progression of prostate cancer by targeting miR-103 through AKT/mTOR signaling pathway. Tumor Biology. 2016;37(12):1–11.

9. Jonathan K, Frampton AE, Reza M, Victoria H, Alex DG, Laura RA, et al. Growth arrest-specific transcript 5 associated snoRNA levels are related to p53 expression and DNA damage in colorectal cancer. Plos One. 2014;9(6):e98561.
10. Gao J, Liu M, Zou Y, Mao M, Shen T, Zhang C, et al. Long non-coding RNA growth arrest-specific transcript 5 is involved in ovarian cancer cell apoptosis through the mitochondria-mediated apoptosis pathway. Oncol Rep. 2015;34(6):3212.
11. Bartel DP. MicroRNAs. Cell. 2004;116(2):0–297.
12. Lim LP, Lau NC, Philip GE, Andrew G, Schelter JM, John C, et al. Microarray analysis shows that some microRNAs downregulate large numbers of target mRNAs. Nature. 2005;433(7027):769–73.
13. Farazi TA, Hoell JI, Morozov P, Tuschl T. MicroRNAs in Human Cancer. Advances in Experimental Medicine Biology. 2013;774(2):1–20.
14. Deb B, Uddin A, Chakraborty S. miRNAs and ovarian cancer: An overview. J Cell Physiol. 2017;233(5):3846–54.
15. Vahabi M, Pulito C, Sacconi A, Donzelli S, D'Andrea M, Manciocco V, et al. miR-96-5p targets PTEN expression affecting radio-chemosensitivity of HNSCC cells. Journal of Experimental Clinical Cancer Research. 2019;38(1):141.
16. Yemin W, Jen-Wei H, Philamer C, Kemp CJ, Toshiyasu T. MiR-96 downregulates REV1 and RAD51 to promote cellular sensitivity to cisplatin and PARP inhibition. Can Res. 2012;72(16):4037–46.
17. Long X, Song K, Hu H, Tian Q, Wang W, Dong Q, et al. Long non-coding RNA GAS5 inhibits DDP-resistance and tumor progression of epithelial ovarian cancer via GAS5-E2F4-PARP1-MAPK axis. J Exp Clin Cancer Res. 2019;38(1):345.
18. Zhou D, Teng F, Verhaak RGW, Zhen S, Yong Z, Myles B, et al. Integrative genomic analyses reveal clinically relevant long noncoding RNAs in human cancer. Nat Struct Mol Biol. 2013;20(7):908–13.
19. Pickard MR, Williams GT. Regulation of apoptosis by long non-coding RNA GAS5 in breast cancer cells: implications for chemotherapy. Breast Cancer Research Treatment. 2014;145(2):359–70.
20. Li J, Huang H, Li Y, Li L, Hou W, You Z. Decreased expression of long non-coding RNA GAS5 promotes cell proliferation, migration and invasion, and indicates a poor prognosis in ovarian cancer. Oncol Rep. 2016;36(6):3241–50.
21. Pickard MR, Williams GT. Molecular and Cellular Mechanisms of Action of Tumour Suppressor GAS5 LncRNA. Genes. 2015;6(3):484–99.
22. Liu B, Wu S, Ma J, Yan S, Xiao Z, Wan L, et al. lncRNA GAS5 Reverses EMT and Tumor Stem Cell-Mediated Gemcitabine Resistance and Metastasis by Targeting miR-221/SOCS3 in Pancreatic Cancer. Mol Ther Nucleic Acids. 2018;13:472–82.
23. Li S, Zhou J, Wang Z, Wang P, Gao X, Wang Y. Long noncoding RNA GAS5 suppresses triple negative breast cancer progression through inhibition of proliferation and invasion by competitively binding miR-196a-5p. Biomed Pharmacother. 2018;104:451–7.

24. Xu C, Zhang Y, Wang Q, Xu Z, Jiang J, Gao Y, et al. Long non-coding RNA GAS5 controls human embryonic stem cell self-renewal by maintaining NODAL signalling. Nat Commun. 2016;7:13287.
25. Dong H, Hu J, Zou K, Ye M, Chen Y, Wu C, et al. Activation of LncRNA TINCR by H3K27 acetylation promotes Trastuzumab resistance and epithelial-mesenchymal transition by targeting MicroRNA-125b in breast Cancer. Molecular Cancer. 2019;18(1):3.
26. Zhao X, Wang P, Liu J, Zheng J, Liu Y, Chen J, et al. Gas5 Exerts Tumor-suppressive Functions in Human Glioma Cells by Targeting miR-222. Mol Ther. 2015;23(12):1899–911.
27. Liang H, Tong Y, Yue H, Hua J, Chengyu W, Tianyi Y, et al. LncRNA PTAR promotes EMT and invasion-metastasis in serous ovarian cancer by competitively binding miR-101-3p to regulate ZEB1 expression. Molecular Cancer. 2018;17(1):119.
28. Wang W, Jia Y-J, Yang Y-L, Xue M, Zheng Z-J, Wang L, et al. LncRNA GAS5 exacerbates renal tubular epithelial fibrosis by acting as a competing endogenous RNA of miR-96-5p. Biomed Pharmacother. 2020;121:109411.
29. Thivierge C, Tseng HW, Mayya VK, Lussier C, Gravel SP, Duchaine TF. Alternative polyadenylation confers Pten mRNAs stability and resistance to microRNAs. Nucleic Acids Res. 2018;46(19):10340–52.
30. Nero C, Ciccarone F, Pietragalla A, Scambia G. PTEN and Gynecological Cancers. Cancers (Basel). 2019;11(10):1458.
31. Xu J, Tian W, Ma X, Guo J, Shi Q, Jin Y, et al. The Molecular Mechanism Underlying Morphine-Induced Akt Activation: Roles of Protein Phosphatases and Reactive Oxygen Species. Cell Biochemistry Biophysics. 2011;61(2):303–11.
32. Jang H, Lee O-H, Lee Y, Yoon H, Chang EM, Park M, et al. Melatonin prevents cisplatin-induced primordial follicle loss via suppression of PTEN/AKT/FOXO3a pathway activation in the mouse ovary. J Pineal Res. 2016;60(3):336–47.
33. Martins FC, Santiago I, Trinh A, Xian J, Guo A, Sayal K, et al. Combined image and genomic analysis of high-grade serous ovarian cancer reveals PTEN loss as a common driver event and prognostic classifier. Genome Biol. 2014;15(12):526.
34. Shao S, Wang C, Wang S, Zhang H, Zhang Y. LncRNA STXBP5-AS1 suppressed cervical cancer progression via targeting miR-96-5p/PTEN axis. Biomed Pharmacother. 2019;117:109082.
35. Kong L, Schäfer G, Bu H, Zhang Y, Zhang Y, Klocker H. Lamin A/C protein is overexpressed in tissue-invading prostate cancer and promotes prostate cancer cell growth, migration and invasion through the PI3K/AKT/PTEN pathway. Carcinogenesis. 2012;33(4):751–9.
36. Kitagishi Y, Matsuda S. Diets involved in PPAR and PI3K/AKT/PTEN pathway may contribute to neuroprotection in a traumatic brain injury. Alzheimers Res Ther. 2013;5(5):42.
37. Patch A-M, Christie EL, Etemadmoghadam D, Garsed DW, George J, Fereday S, et al. Whole-genome characterization of chemoresistant ovarian cancer. Nature. 2015;521(7553):489–94.
38. Russo A, Czarnecki AA, Dean M, Modi DA, Lantvit DD, Hardy L, et al. PTEN loss in the fallopian tube induces hyperplasia and ovarian tumor formation. Oncogene. 2018;37(15):1976–90.

39. Zeng B, Li Y, Jiang F, Wei C, Chen G, Zhang W, et al. LncRNA GAS5 suppresses proliferation, migration, invasion, and epithelial-mesenchymal transition in oral squamous cell carcinoma by regulating the miR-21/PTEN axis. Exp Cell Res. 2019;374(2):365–73.

Figures

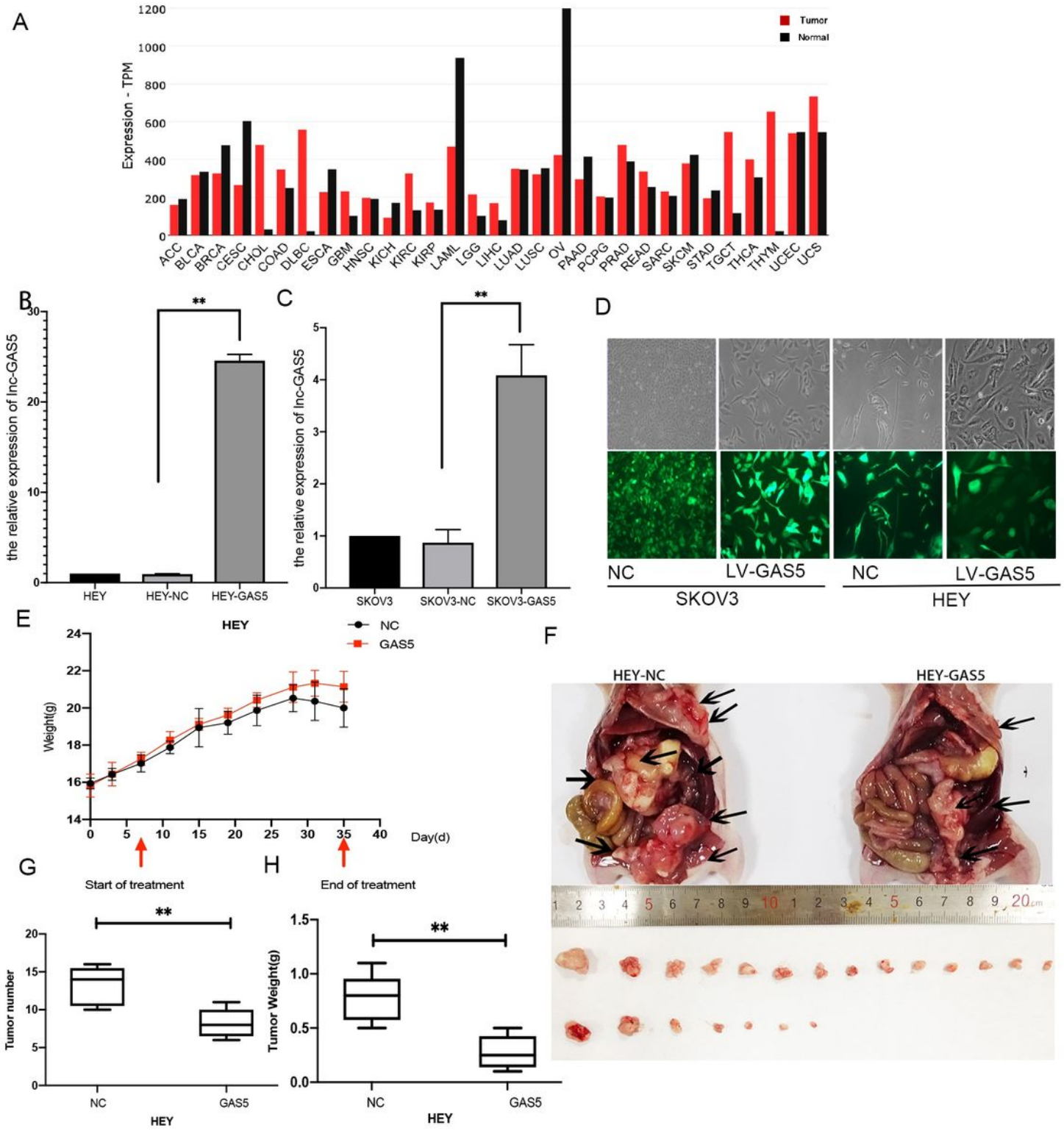

Figure 1

lncRNA GAS5 is downregulated in OC and inhibits OC tumor growth in mouse xenograft models. (A) GAS5 had a low-level expression in ovarian cancer (OC). (B-C) LV-GAS5 or the empty LV vector plasmids were transfected into OC cells. After 72 h, overexpression efficiency of GAS5 was evaluated by real-time quantitative PCR (real-time qPCR). (D) Following stable transfection of mutation type GAS5 (GAS5 Mut) plasmid (200 ×). (E) Body weight was monitored during the detectable period in nude mice. (F) Typical images of disseminated tumors in intraperitoneal OC xenograft model treated with vehicle NC buffer or LV-GAS5. (G-H) Whole tumor number and weight in intraperitoneal OC xenograft model treated with vehicle NC buffer (n = 6) or LV-GAS5 (n = 6) were quantified in nude mice. *, $P < 0.05$; **, $P < 0.01$.

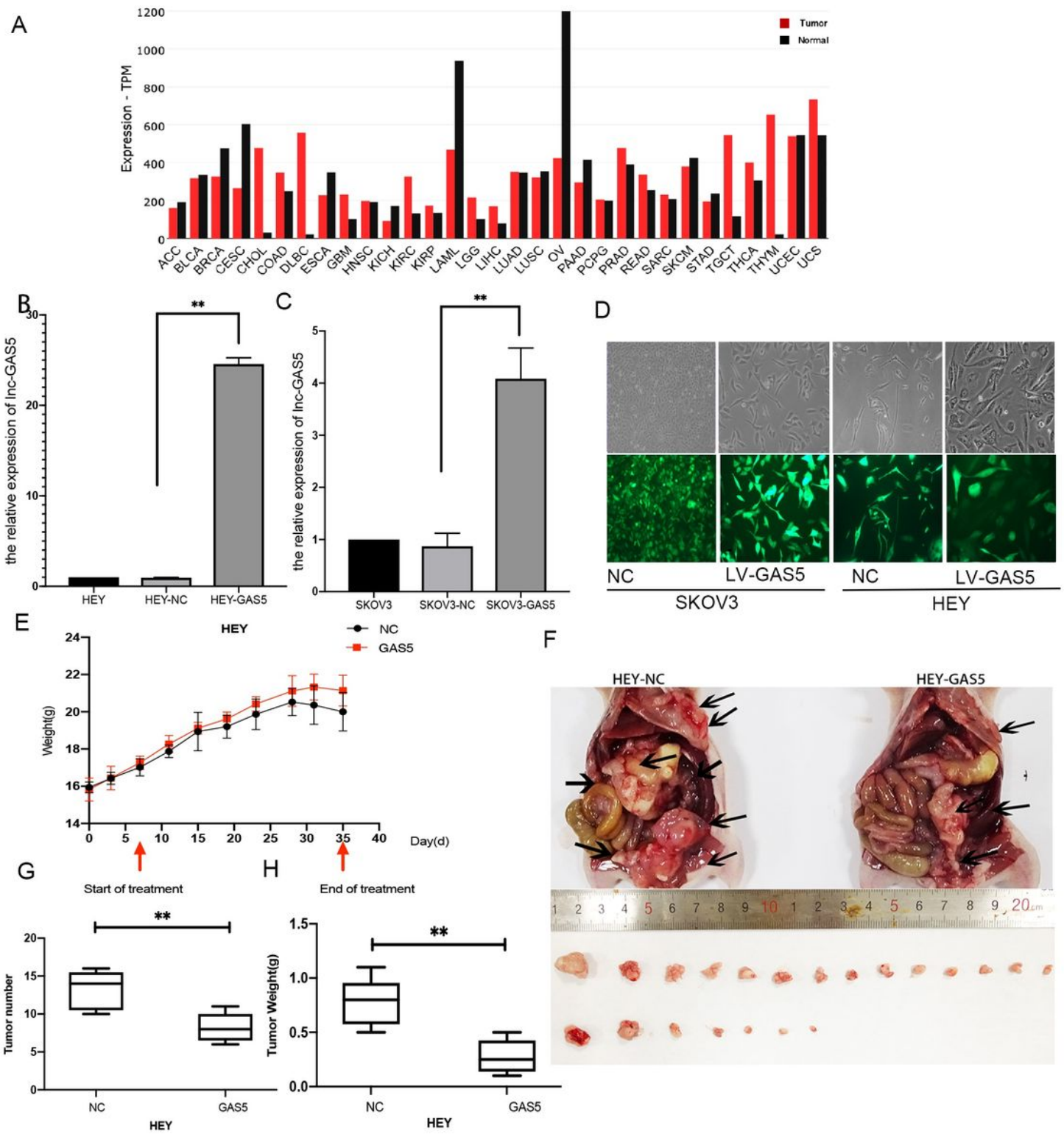

Figure 1

lncRNA GAS5 is downregulated in OC and inhibits OC tumor growth in mouse xenograft models. (A) GAS5 had a low-level expression in ovarian cancer (OC). (B-C) LV-GAS5 or the empty LV vector plasmids were transfected into OC cells. After 72 h, overexpression efficiency of GAS5 was evaluated by real-time quantitative PCR (real-time qPCR). (D) Following stable transfection of mutation type GAS5 (GAS5 Mut) plasmid (200 ×). (E) Body weight was monitored during the detectable period in nude mice. (F) Typical

images of disseminated tumors in intraperitoneal OC xenograft model treated with vehicle NC buffer or LV-GAS5. (G-H) Whole tumor number and weight in intraperitoneal OC xenograft model treated with vehicle NC buffer (n = 6) or LV-GAS5 (n = 6) were quantified in nude mice. *, P < 0.05; **, P < 0.01.

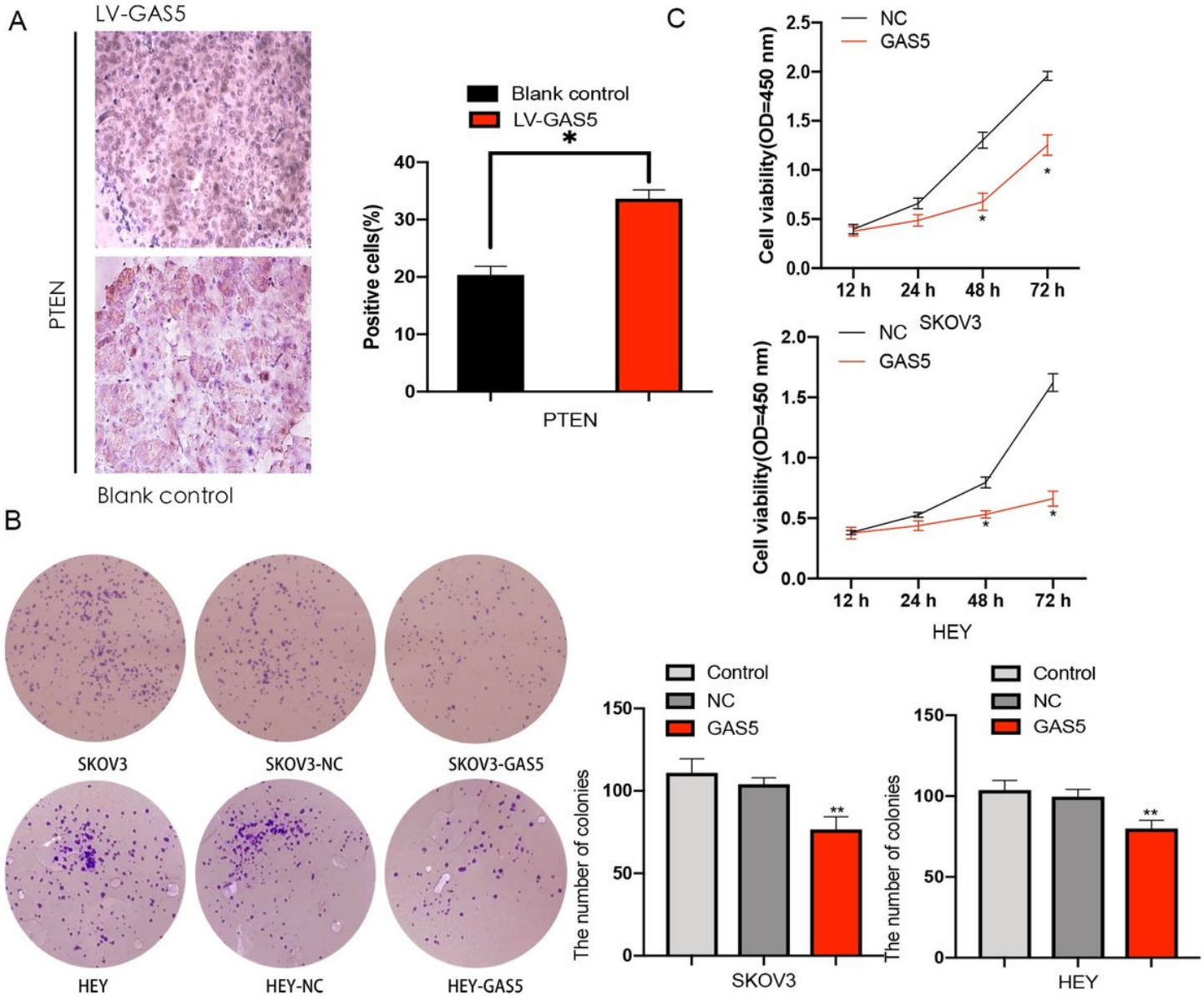

Figure 2

lncRNA GAS5 suppresses HEY and SKOV3 cell proliferation ability (A) Tumor tissues in nude mice were detected PTEN expression according to immunohistochemical staining. (B) Proliferation of HEY and SKOV3 cell lines were compared between LV-GAS5 and NC groups. (C)Viability of HEY and SKOV3 cell lines in LV-GAS5 and NC groups was assessed. The experiments were repeated thrice. Data are shown as percent control of vehicle-treated wells. *, P < 0.05; **, P < 0.01□***, P < 0.001.

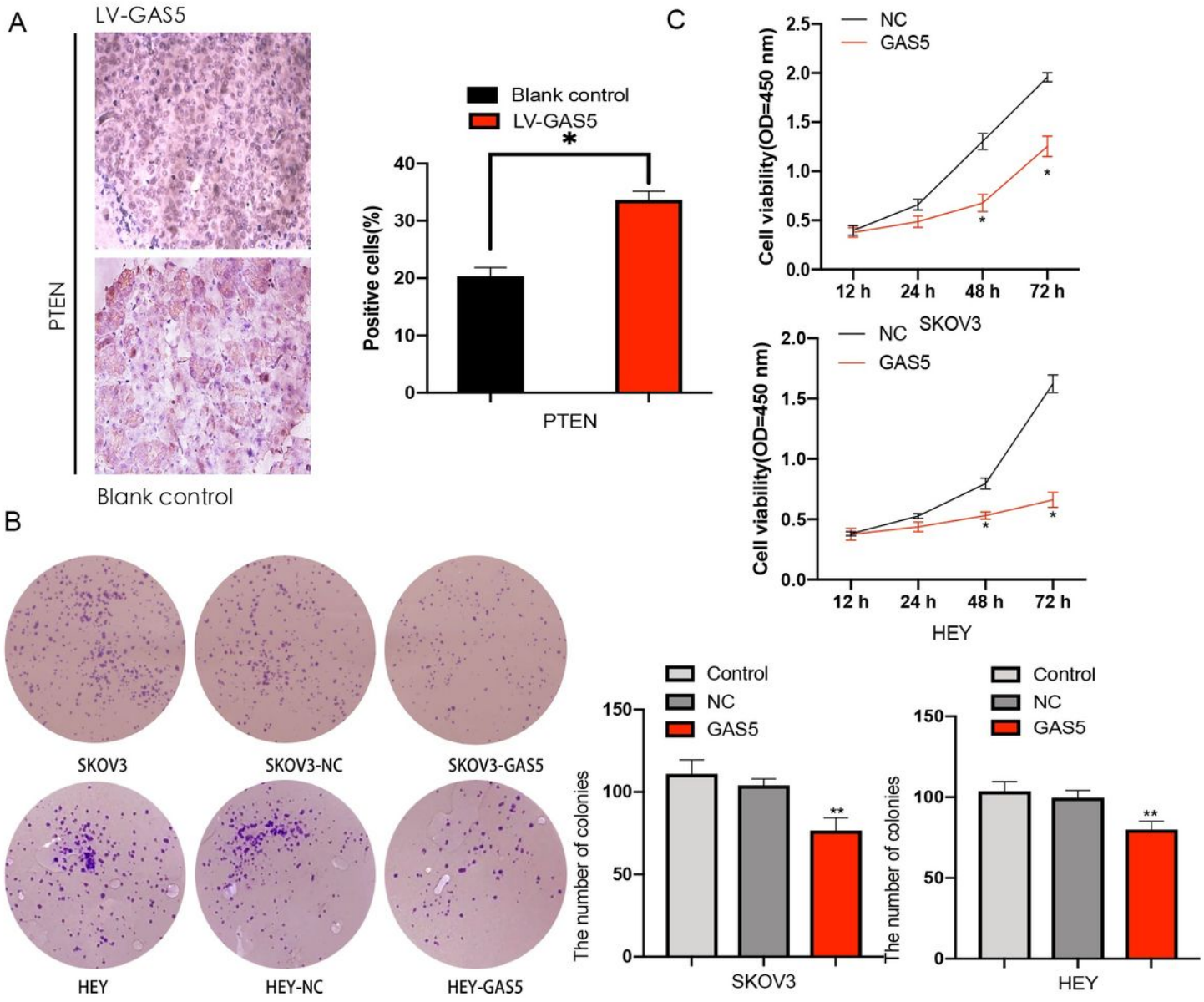

Figure 2

lncRNA GAS5 suppresses HEY and SKOV3 cell proliferation ability (A) Tumor tissues in nude mice were detected PTEN expression according to immunohistochemical staining. (B) Proliferation of HEY and SKOV3 cell lines were compared between LV-GAS5 and NC groups. (C)Viability of HEY and SKOV3 cell lines in LV-GAS5 and NC groups was assessed. The experiments were repeated thrice. Data are shown as percent control of vehicle-treated wells. *, P < 0.05; **, P < 0.01；***, P < 0.001.

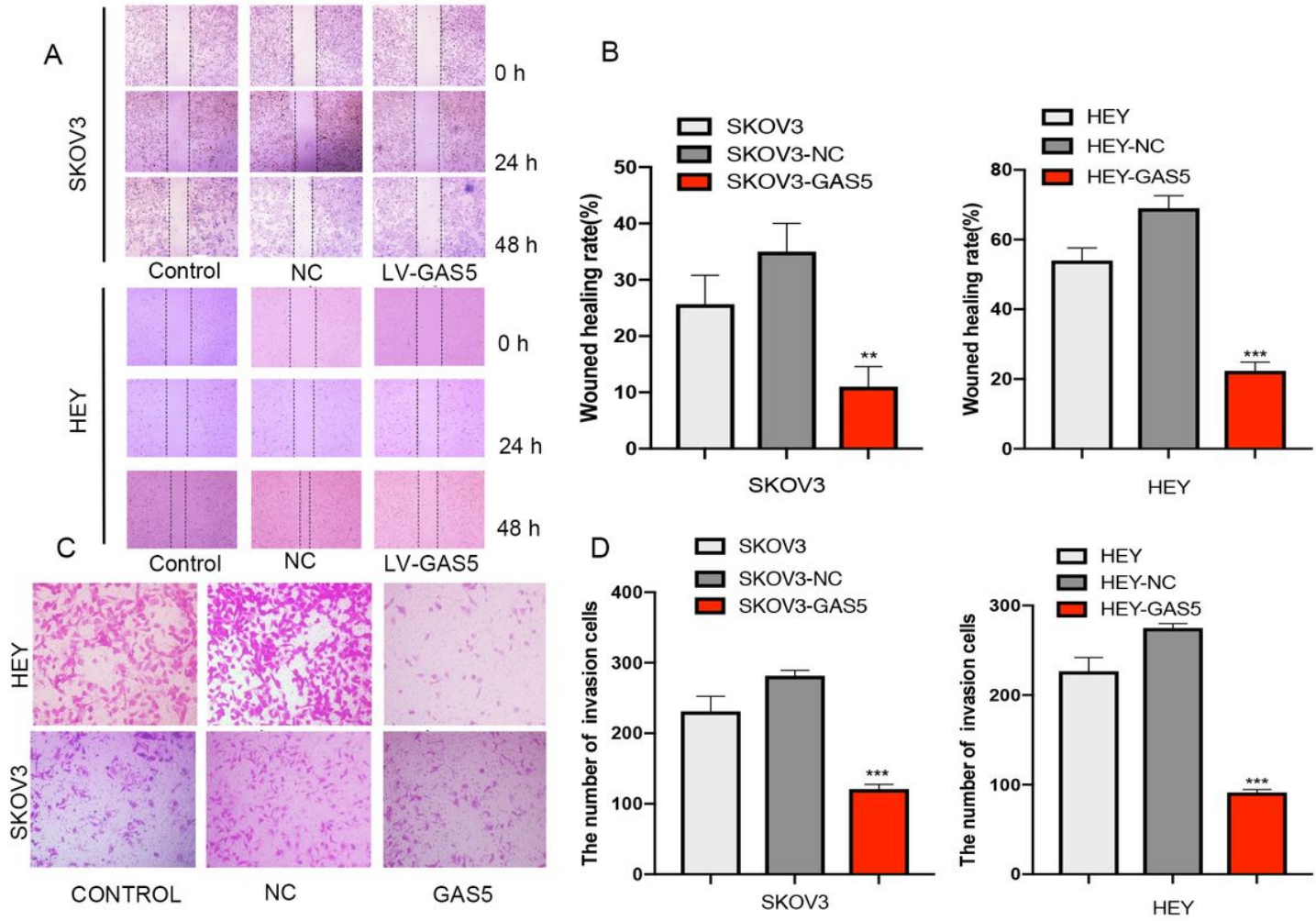

Figure 3

lncRNA GAS5 suppresses HEY and SKOV3 cell migration and invasion ability (A) A wound-healing test was conducted to examine the migration of HEY and SKOV3 cells in the seven groups at 24 h and 48 h following transfection. (B) The wound-healing rate in HEY and SKOV3 cells. GAS5 compared with the control group. (C) The cell invasion of HEY and SKOV3 cells following transfection in GAS5 and NC groups (200 ×). (D) The number of invasive HEY and SKOV3 cells following transfection in the oe-GAS5 group. The data are presented as the mean ± standard deviation (SD) and analyzed by one-way analysis of variance (ANOVA). The experiment was independently repeated thrice. *, P < 0.05.

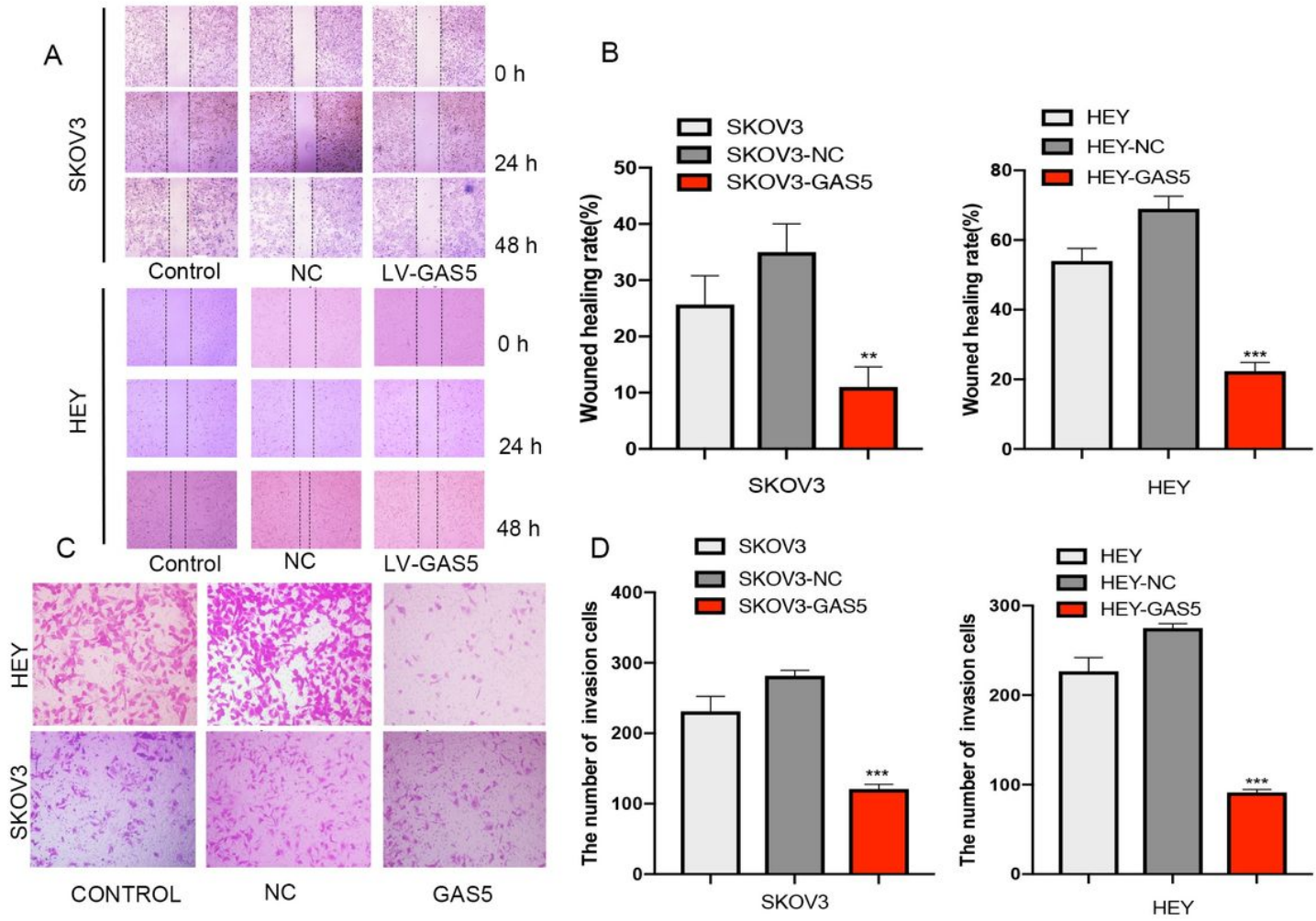

Figure 3

lncRNA GAS5 suppresses HEY and SKOV3 cell migration and invasion ability (A) A wound-healing test was conducted to examine the migration of HEY and SKOV3 cells in the seven groups at 24 h and 48 h following transfection. (B) The wound-healing rate in HEY and SKOV3 cells. GAS5 compared with the control group. (C) The cell invasion of HEY and SKOV3 cells following transfection in GAS5 and NC groups (200 ×). (D) The number of invasive HEY and SKOV3 cells following transfection in the oe-GAS5 group. The data are presented as the mean ± standard deviation (SD) and analyzed by one-way analysis of variance (ANOVA). The experiment was independently repeated thrice. *, P < 0.05.

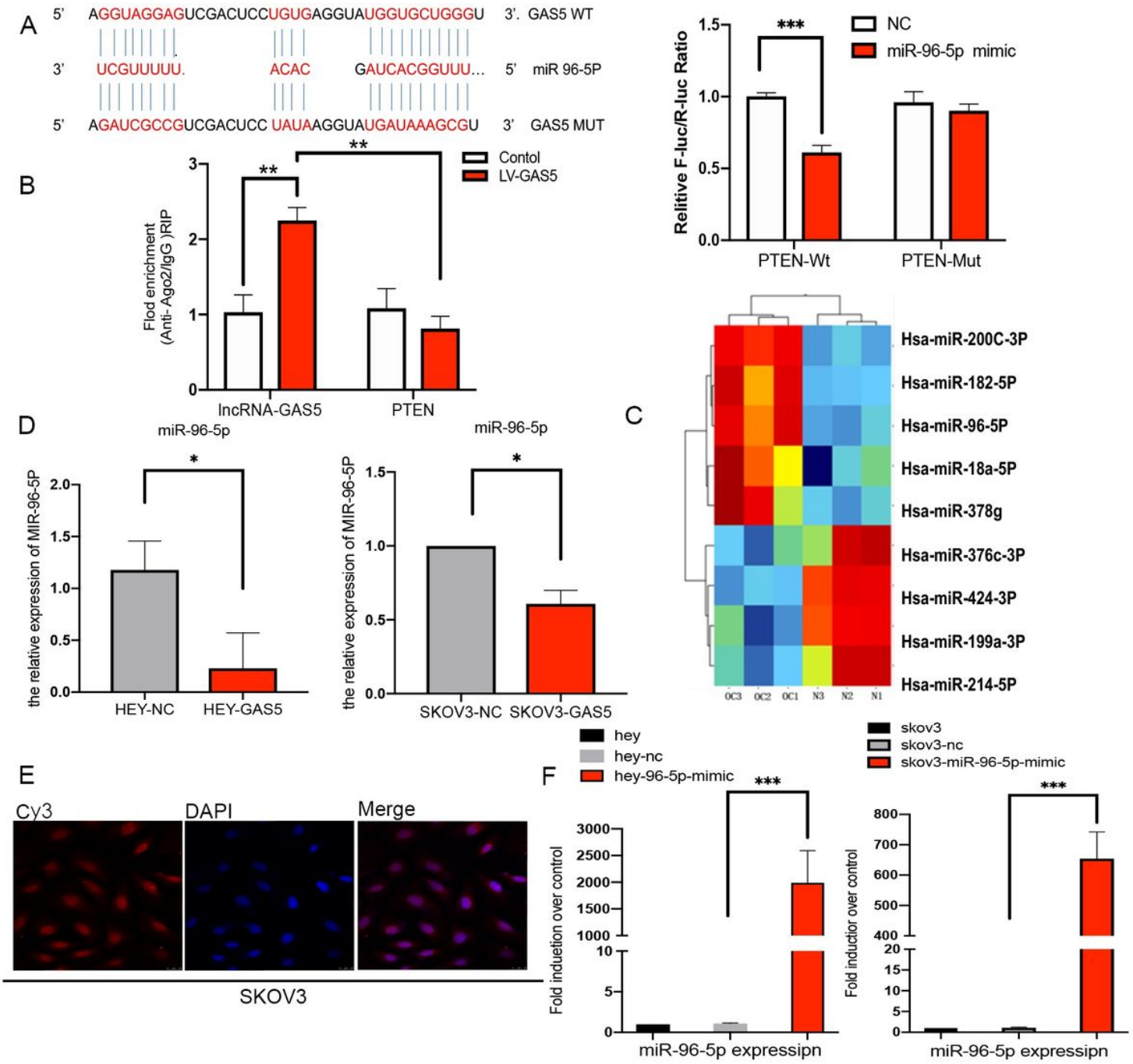

Figure 4

lncRNA GAS5 sponged miR-96-5p by direct targeting (A) The miR-96-5p binding site in lnc-GAS5 3′ UTR. Binding relationship between GAS5 and miR-96-5p was detected by luciferase reporter assay with wild-type (WT) or Mut luciferase reporter plasmids of GAS5. (B) qPCR results of the RIP showed lncRNA GAS5 can compete with PTEN by binding Ago2 protein. (C) Heatmap showing the hierarchical clustering of differentially expressed genes in patients with GAS5. Red: upregulated genes; green: downregulated genes. (D) miR-96-5p expression was detected by real-time qPCR. OC cell lines were transfected with LV-GAS5 (E) FISH assay revealed that lnc-GAS5 was localized in the cytoplasm and the nucleus of SKOV3

cells. (F) miR-96-5p expression was assessed by real-time qPCR when miR-96-5p mimic was transfected in HEY and SKOV3 cell lines. *, P < 0.05; **, P < 0.01；***, P < 0.001.

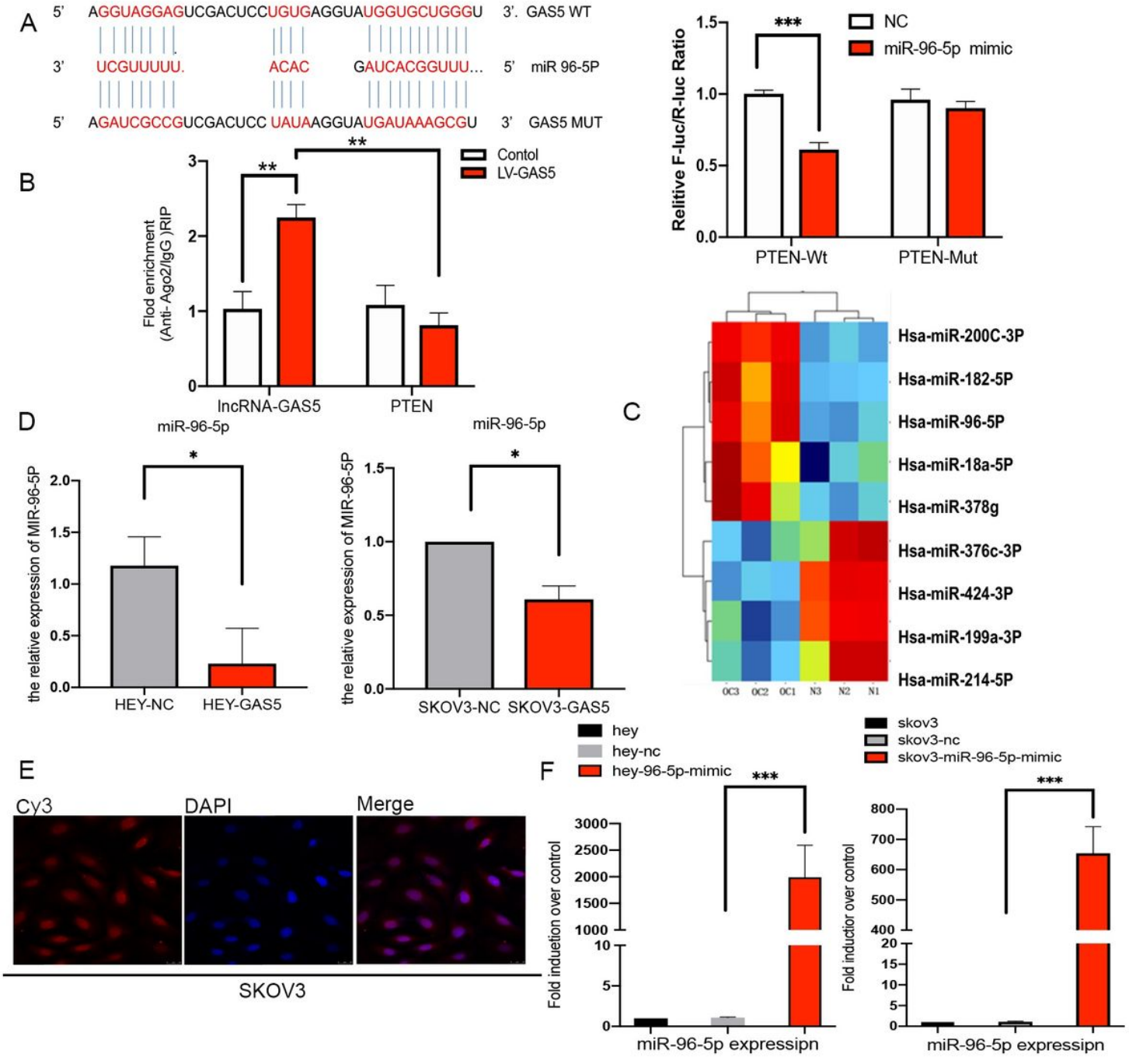

Figure 4

lncRNA GAS5 sponged miR-96-5p by direct targeting (A) The miR-96-5p binding site in lnc-GAS5 3′ UTR. Binding relationship between GAS5 and miR-96-5p was detected by luciferase reporter assay with wild-type (WT) or Mut luciferase reporter plasmids of GAS5. (B) qPCR results of the RIP showed lncRNA GAS5 can compete with PTEN by binding Ago2 protein. (C) Heatmap showing the hierarchical clustering of differentially expressed genes in patients with GAS5. Red: upregulated genes; green: downregulated genes. (D) miR-96-5p expression was detected by real-time qPCR. OC cell lines were transfected with LV-

GAS5 (E) FISH assay revealed that lnc-GAS5 was localized in the cytoplasm and the nucleus of SKOV3 cells. (F) miR-96-5p expression was assessed by real-time qPCR when miR-96-5p mimic was transfected in HEY and SKOV3 cell lines. *, P < 0.05; **, P < 0.01；***, P < 0.001.

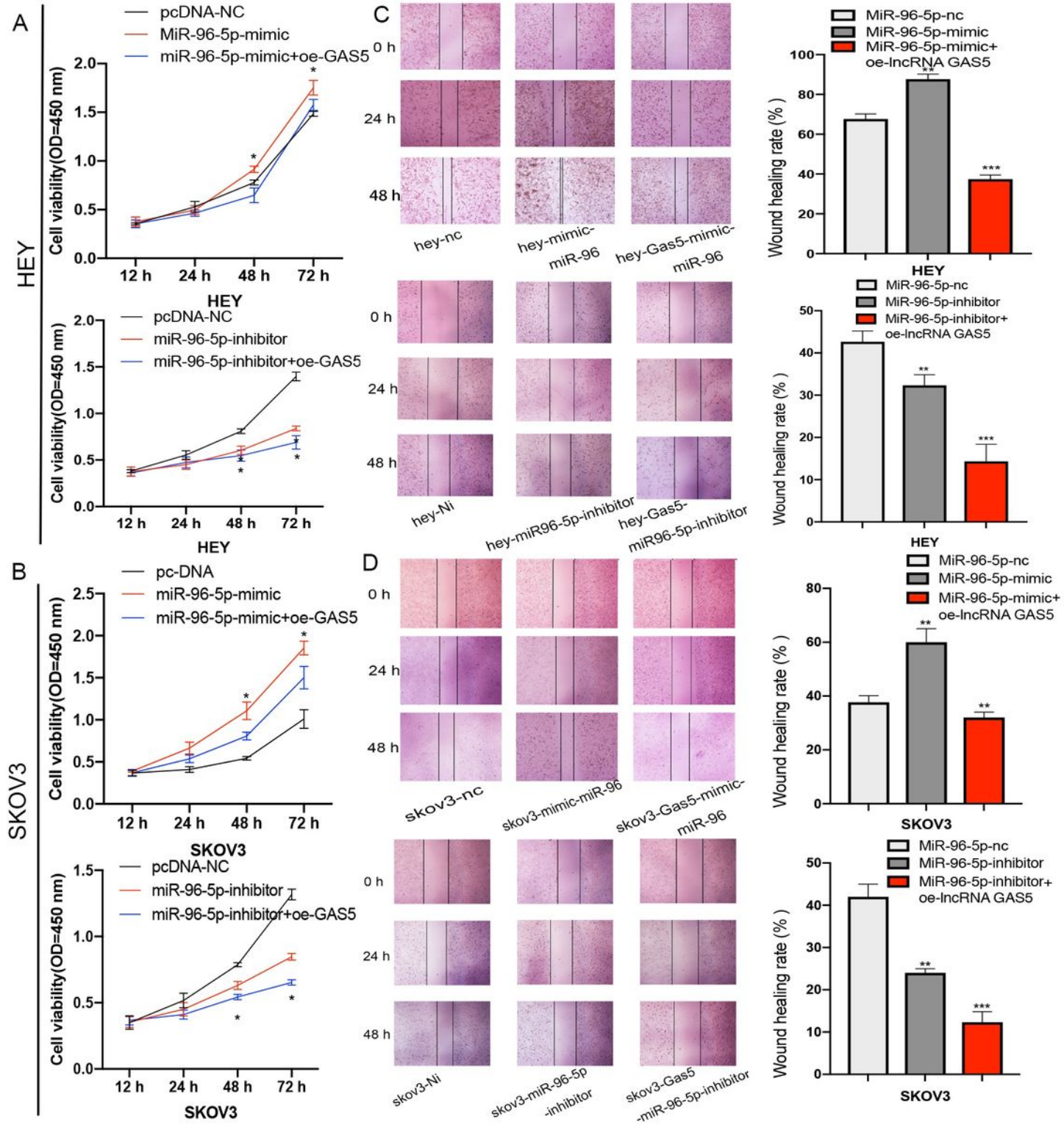

Figure 5

lncRNA GAS5 inhibits HEY and SKOV3 cell Viability and migration ability through the modulation of miR-96-5p. (A-B) Viability of HEY and SKOV3 cell lines was assessed with in LV-GAS5, miR-96-5p mimic, miR-

96-5p inhibitor, and NC groups. (C-D) A wound-healing test was conducted to examine the migration of HEY cells and SKOV3 cells in the three groups at 24 and 48 h following transfection. The data are presented as the mean ± SD and analyzed using one-way ANOVA. The experiment was independently repeated thrice. *, P < 0.05; **, P < 0.01；***, P < 0.001.

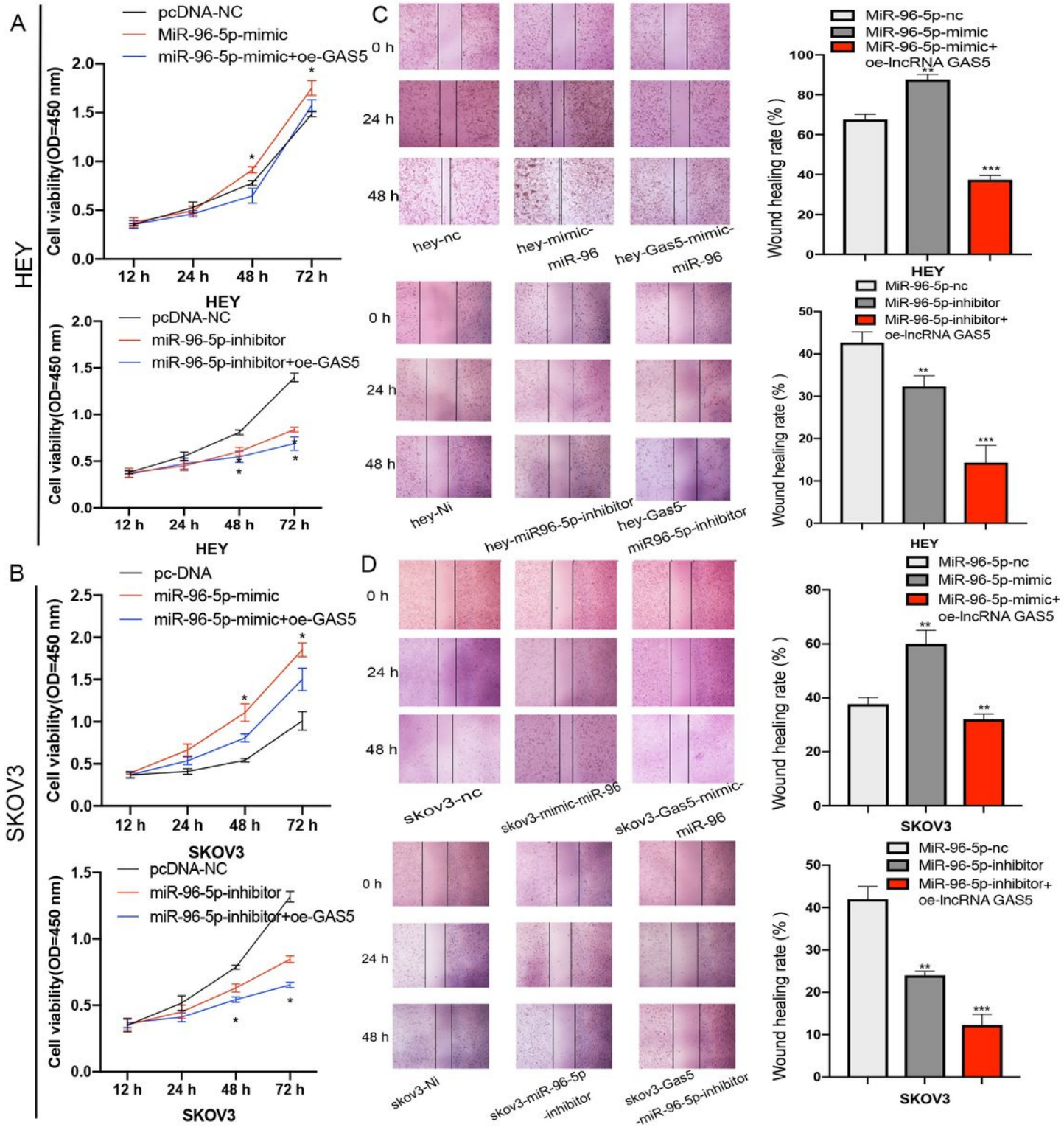

Figure 5

lncRNA GAS5 inhibits HEY and SKOV3 cell Viability and migration ability through the modulation of miR-96-5p. (A-B) Viability of HEY and SKOV3 cell lines was assessed with in LV-GAS5, miR-96-5p mimic, miR-96-5p inhibitor, and NC groups. (C-D) A wound-healing test was conducted to examine the migration of HEY cells and SKOV3 cells in the three groups at 24 and 48 h following transfection. The data are presented as the mean ± SD and analyzed using one-way ANOVA. The experiment was independently repeated thrice. *, P < 0.05; **, P < 0.01；***, P < 0.001.

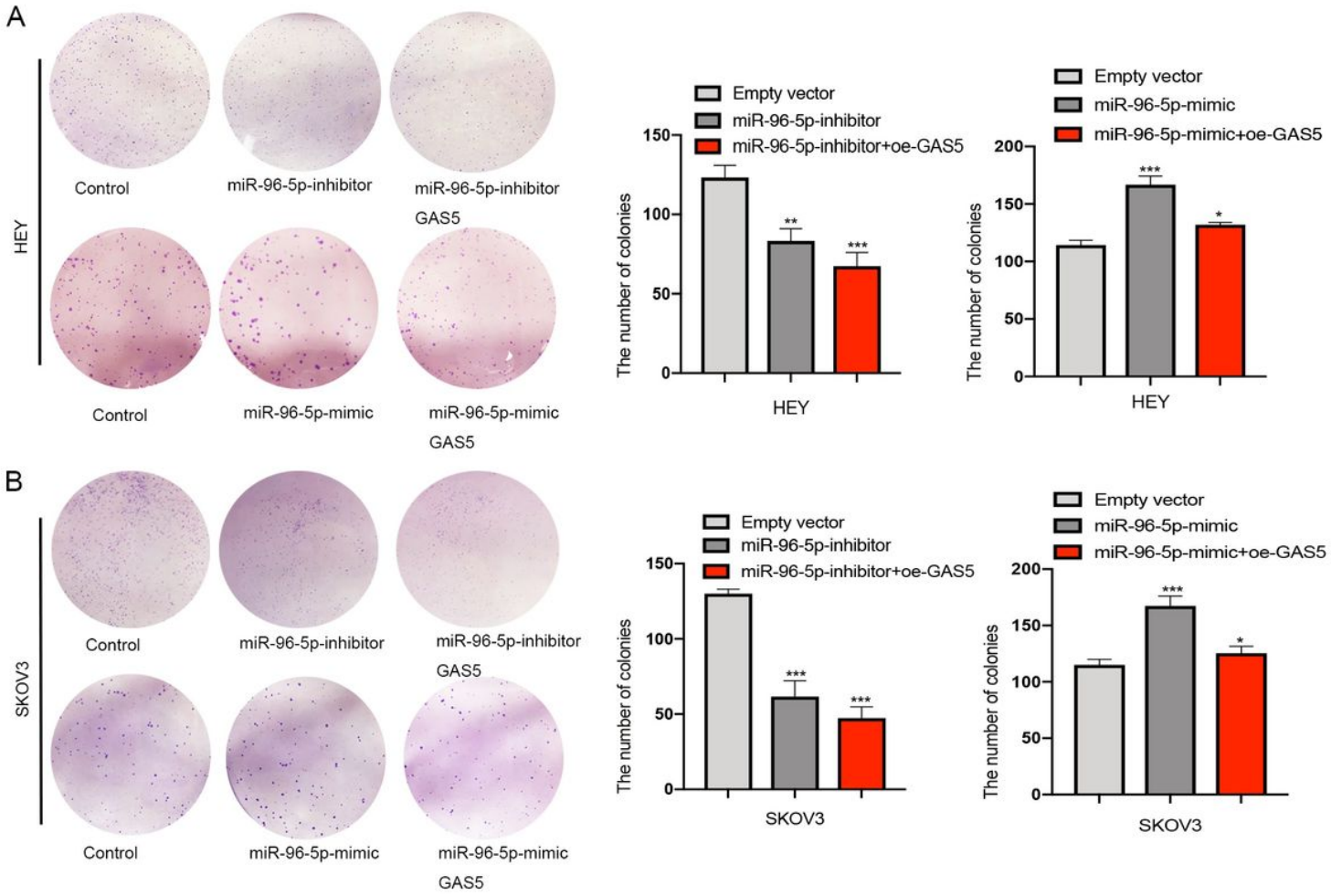

Figure 6

lncRNA GAS5 inhibits HEY and SKOV3 cell proliferation ability through the modulation of miR-96-5p. (A-B) Proliferation of HEY and SKOV3 cell lines were assessed in LV-GAS5, miR-96-5pmimic, miR-96-5p inhibitor, and NC groups. The data are presented as the mean ± SD and analyzed using one-way ANOVA. The experiment was independently repeated thrice. *, P < 0.05.; **, P < 0.01；***, P < 0.001.

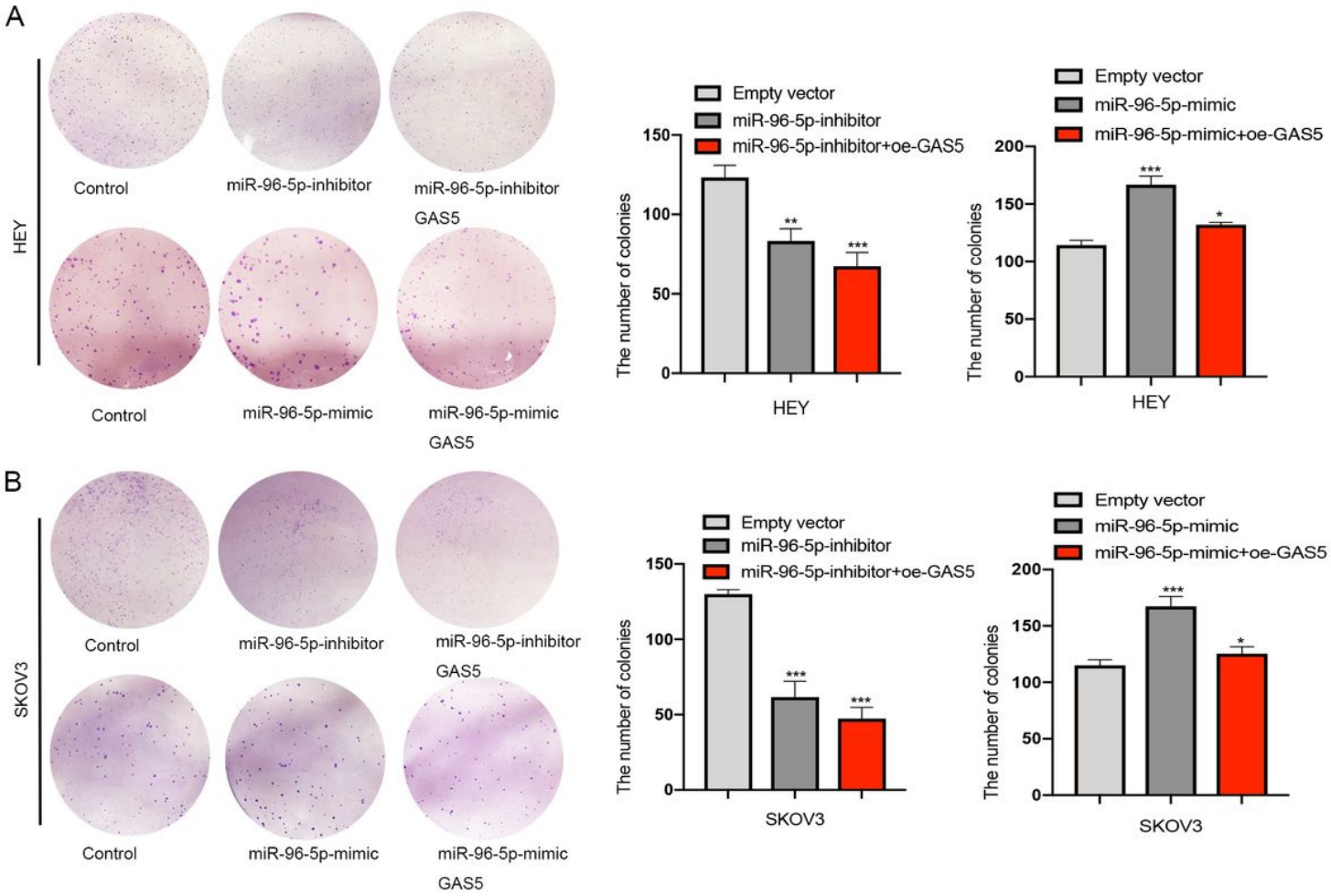

Figure 6

lncRNA GAS5 inhibits HEY and SKOV3 cell proliferation ability through the modulation of miR-96-5p. (A-B) Proliferation of HEY and SKOV3 cell lines were assessed in LV-GAS5, miR-96-5pmimic, miR-96-5p inhibitor, and NC groups. The data are presented as the mean ± SD and analyzed using one-way ANOVA. The experiment was independently repeated thrice. *, P < 0.05.; **, P < 0.01；***, P < 0.001.

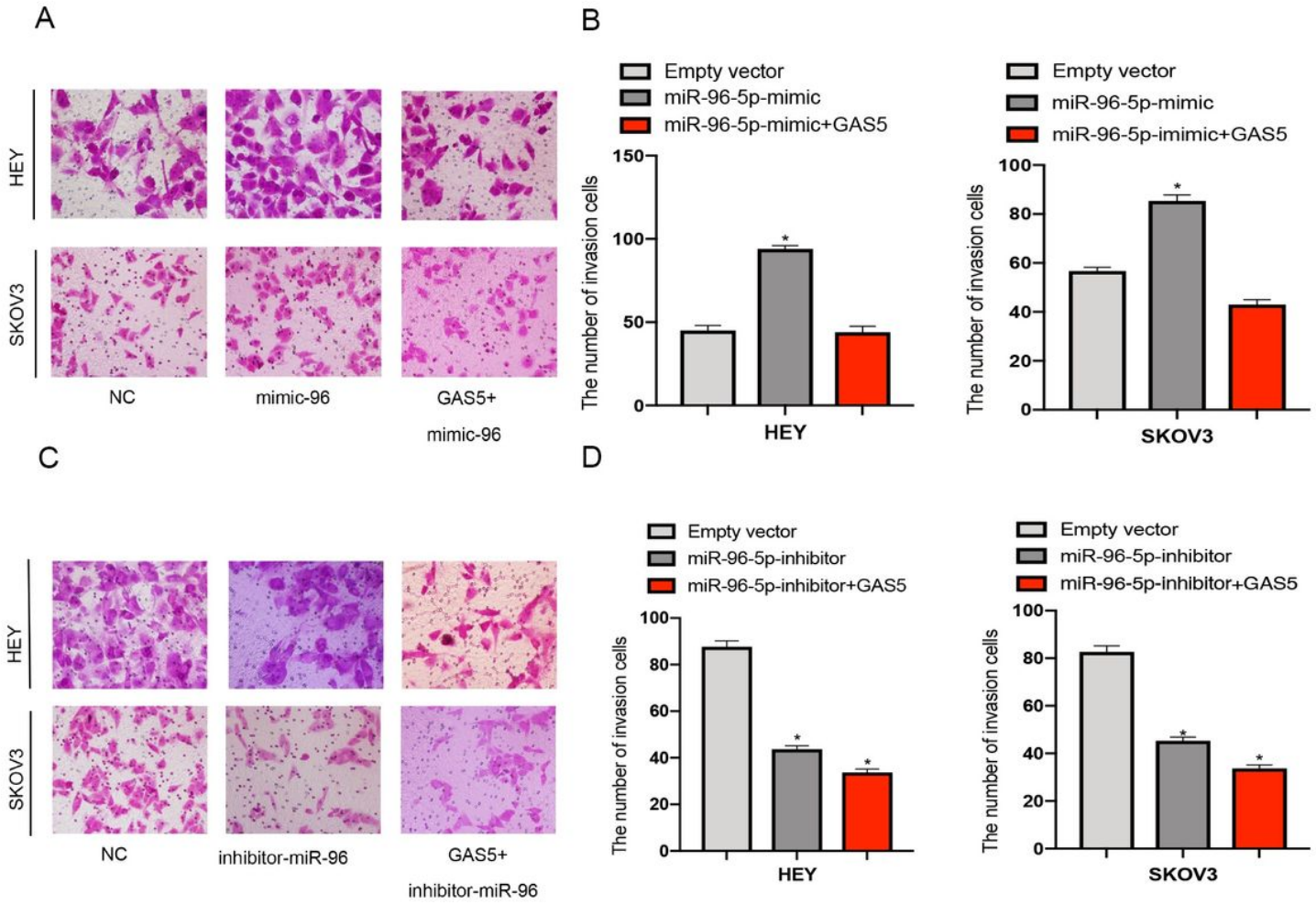

Figure 7

lncRNA GAS5 inhibits HEY and SKOV3 cells invasion ability through the modulation of miR-96-5p. (A) Transwell assay of HEY and SKOV3 cells in LV-GAS5 and miR-96-5p mimic groups after transfection (200 ×). (B) The number of invasive HEY and SKOV3 cells in LV-GAS5 and miR-96-5p mimic groups after transfection. (C) Transwell assay of HEY and SKOV3 cells in the miR-96-5p inhibitor group after transfection (200 ×). (D) The number of invasive HEY and SKOV3 cells in LV-GAS5 and miR-96-5p inhibitor groups following transfection. The data are presented as the mean ± SD and analyzed using one-way ANOVA. The experiment was independently repeated thrice. *, $P < 0.05$.

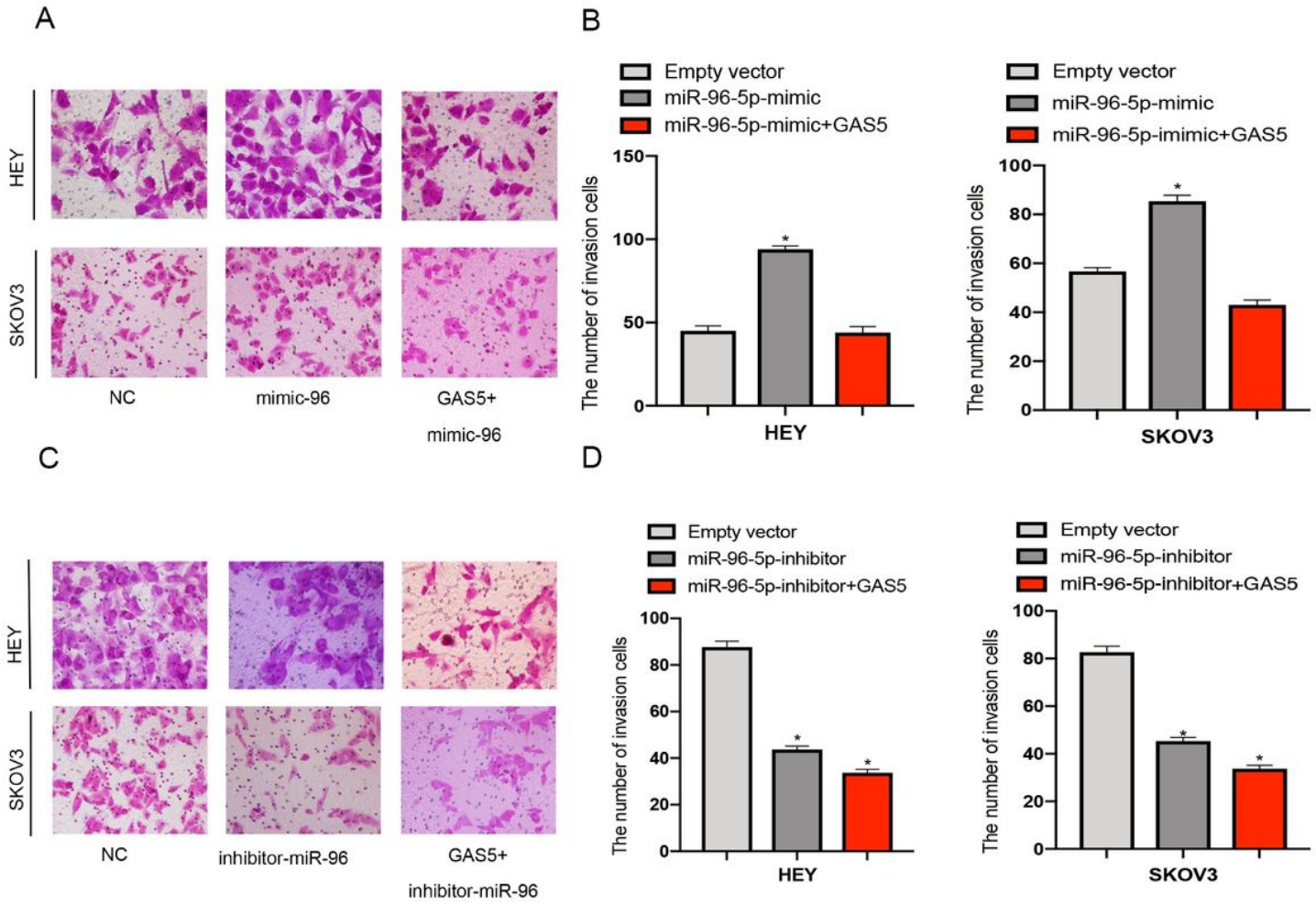

Figure 7

lncRNA GAS5 inhibits HEY and SKOV3 cells invasion ability through the modulation of miR-96-5p. (A) Transwell assay of HEY and SKOV3 cells in LV-GAS5 and miR-96-5p mimic groups after transfection (200 ×). (B) The number of invasive HEY and SKOV3 cells in LV-GAS5 and miR-96-5p mimic groups after transfection. (C) Transwell assay of HEY and SKOV3 cells in the miR-96-5p inhibitor group after transfection (200 ×). (D) The number of invasive HEY and SKOV3 cells in LV-GAS5 and miR-96-5p inhibitor groups following transfection. The data are presented as the mean ± SD and analyzed using one-way ANOVA. The experiment was independently repeated thrice. *, $P < 0.05$.

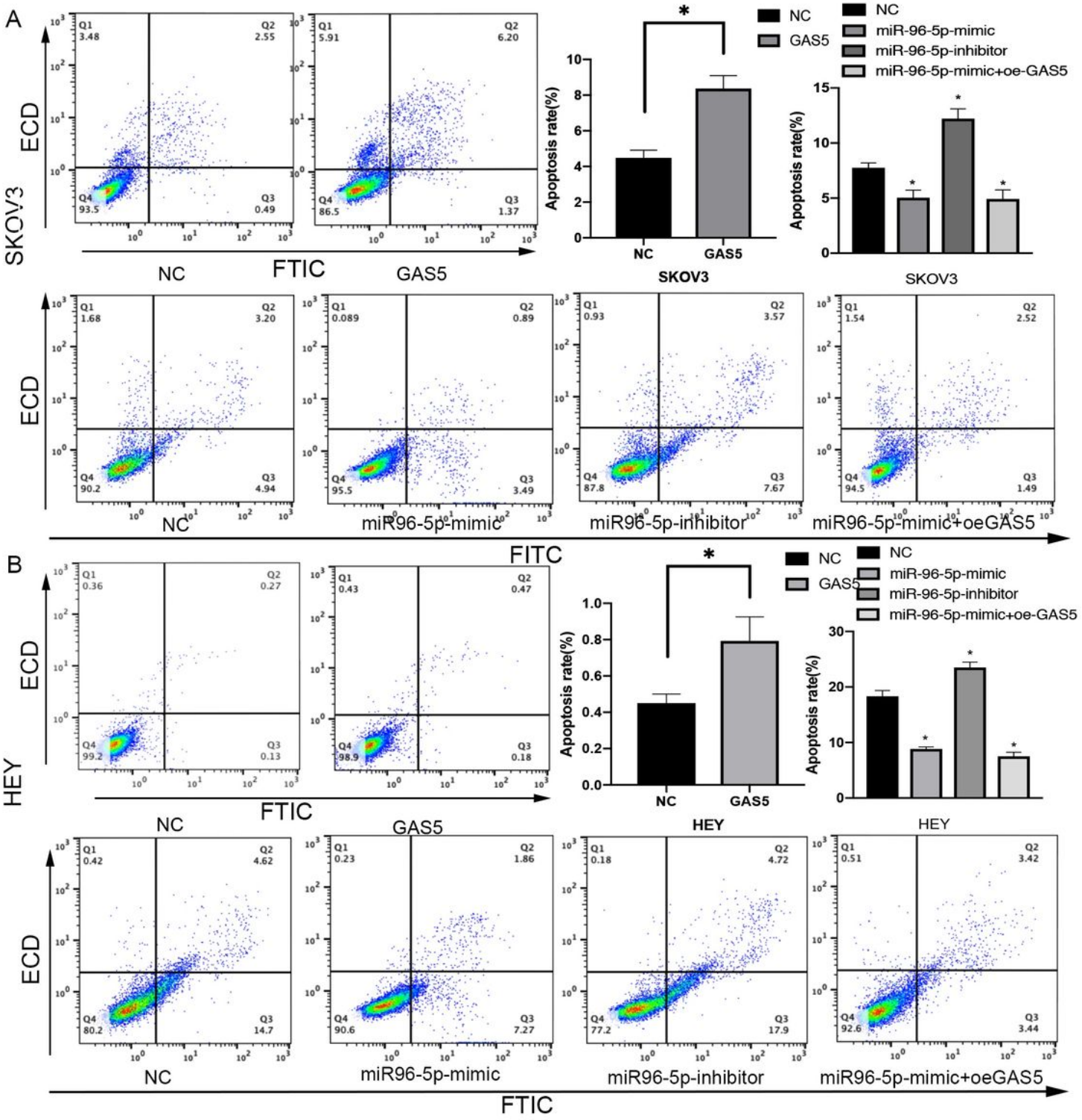

Figure 8

lncRNA GAS5 promotes HEY and SKOV3 cell apoptosis through the modulation of miR-96-5p. (A) SKOV3 cell apoptosis at 48 h post treatment, measured by flow cytometry. Apoptosis rate in LV-GAS5, miR-96-5p mimic, and LV-GAS5+ miR-96-5p mimic, and miR-96-5p inhibitor groups. (B) HEY cell apoptosis at 48 h post treatment measured by flow cytometry. Apoptosis rate in LV-GAS5, miR-96-5p mimic, and LV-GAS5+

miR-96-5p mimic, and miR-96-5p inhibitor groups. The data are presented as the mean ± SD and analyzed using one-way ANOVA. The experiment was independently repeated thrice. *, P < 0.05.

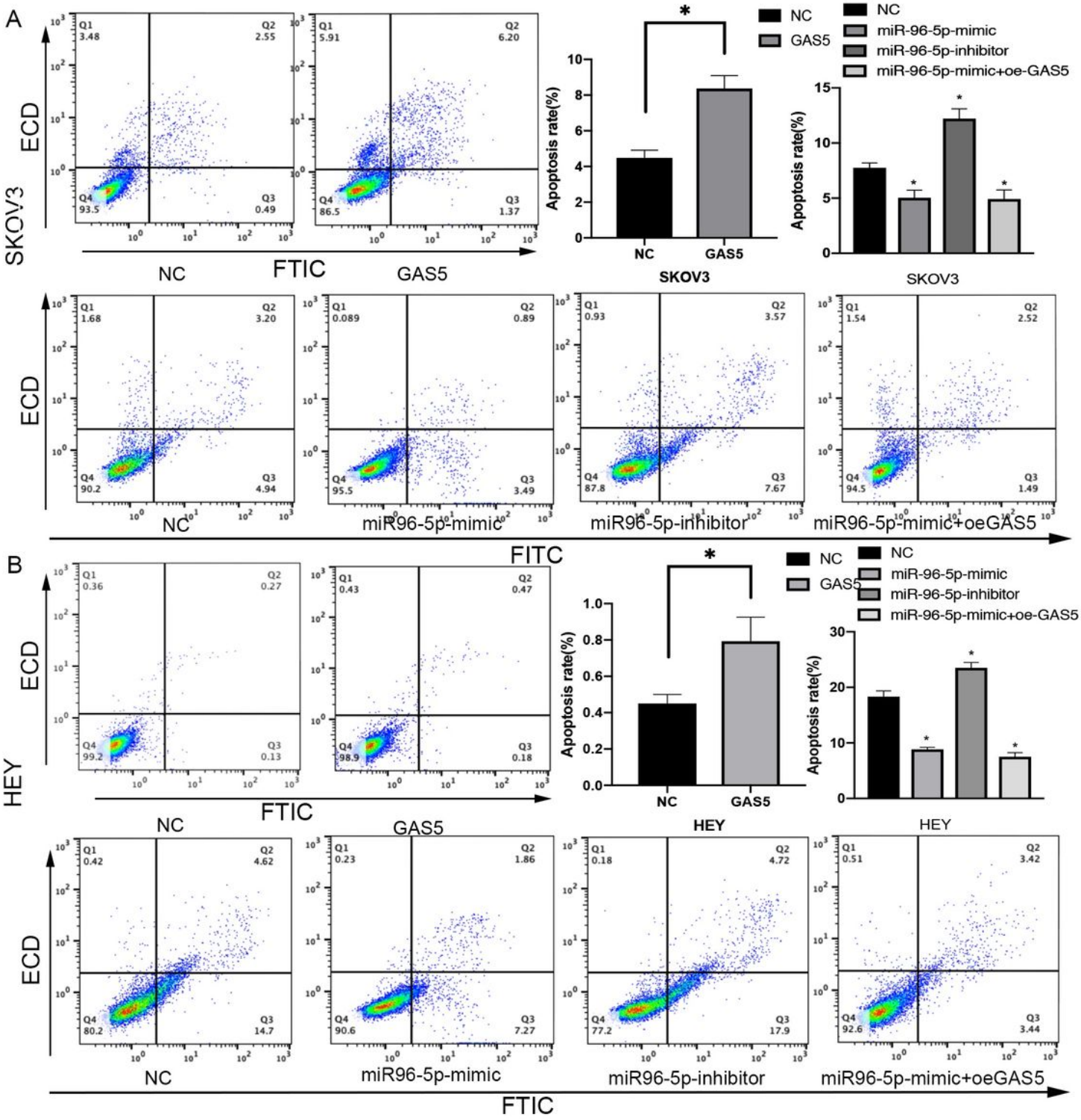

Figure 8

lncRNA GAS5 promotes HEY and SKOV3 cell apoptosis through the modulation of miR-96-5p. (A) SKOV3 cell apoptosis at 48 h post treatment, measured by flow cytometry. Apoptosis rate in LV-GAS5, miR-96-5p mimic, and LV-GAS5+ miR-96-5p mimic, and miR-96-5p inhibitor groups. (B) HEY cell apoptosis at 48 h

post treatment measured by flow cytometry. Apoptosis rate in LV-GAS5, miR-96-5p mimic, and LV-GAS5+ miR-96-5p mimic, and miR-96-5p inhibitor groups. The data are presented as the mean ± SD and analyzed using one-way ANOVA. The experiment was independently repeated thrice. *, P < 0.05.

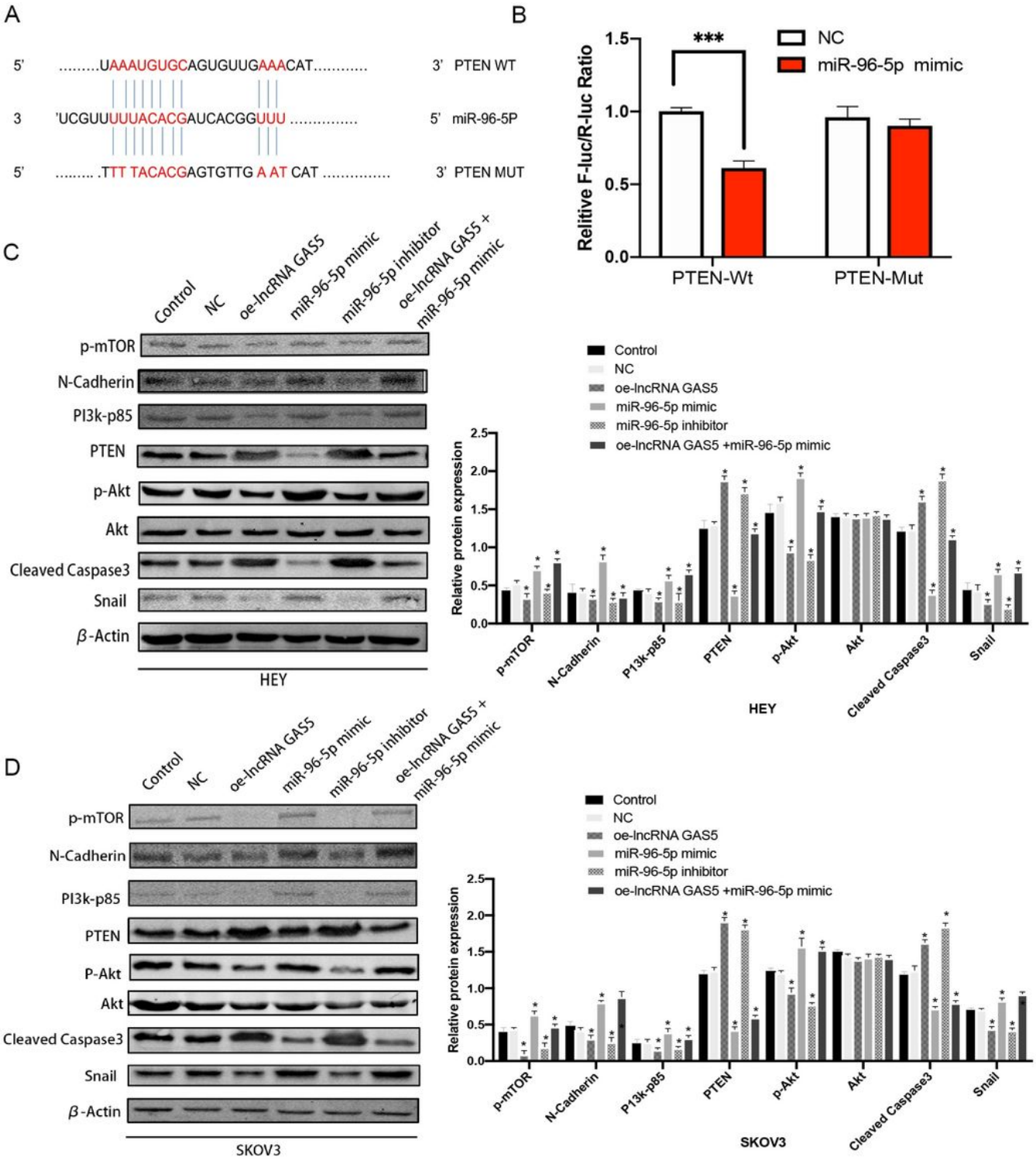

Figure 9

lncRNA GAS5 increases protein levels of PTEN and cleaved caspase-3 but decreases the phosphorylation of AKT, mTOR, N-cadherin and Snail. (A) The miR-96-5p binding site in the sequence of PTEN 3′ UTR. (B)

Binding relationship between PTEN and miR-96-5p was detected by luciferase reporter assay with WT or Mut luciferase reporter plasmids of PTEN. (C) The protein bands of P-mTOR, N-cadherin, PI3K-p85, PTEN, AKT, p-AKT, cleaved caspase-3, Snail, and β-actin in HEY cells detected by western blot assay. (D) The protein bands of P-mTOR, N-cadherin, PI3K-p85, PTEN, AKT, P-AKT, cleaved caspase-3, Snail, and β-actin in SKOV3 cells detected by western blot. The data are presented as the mean ± SD and analyzed using one-way ANOVA. The experiment was independently repeated thrice. *, P < 0.05; **, P < 0.01；***, P < 0.001.

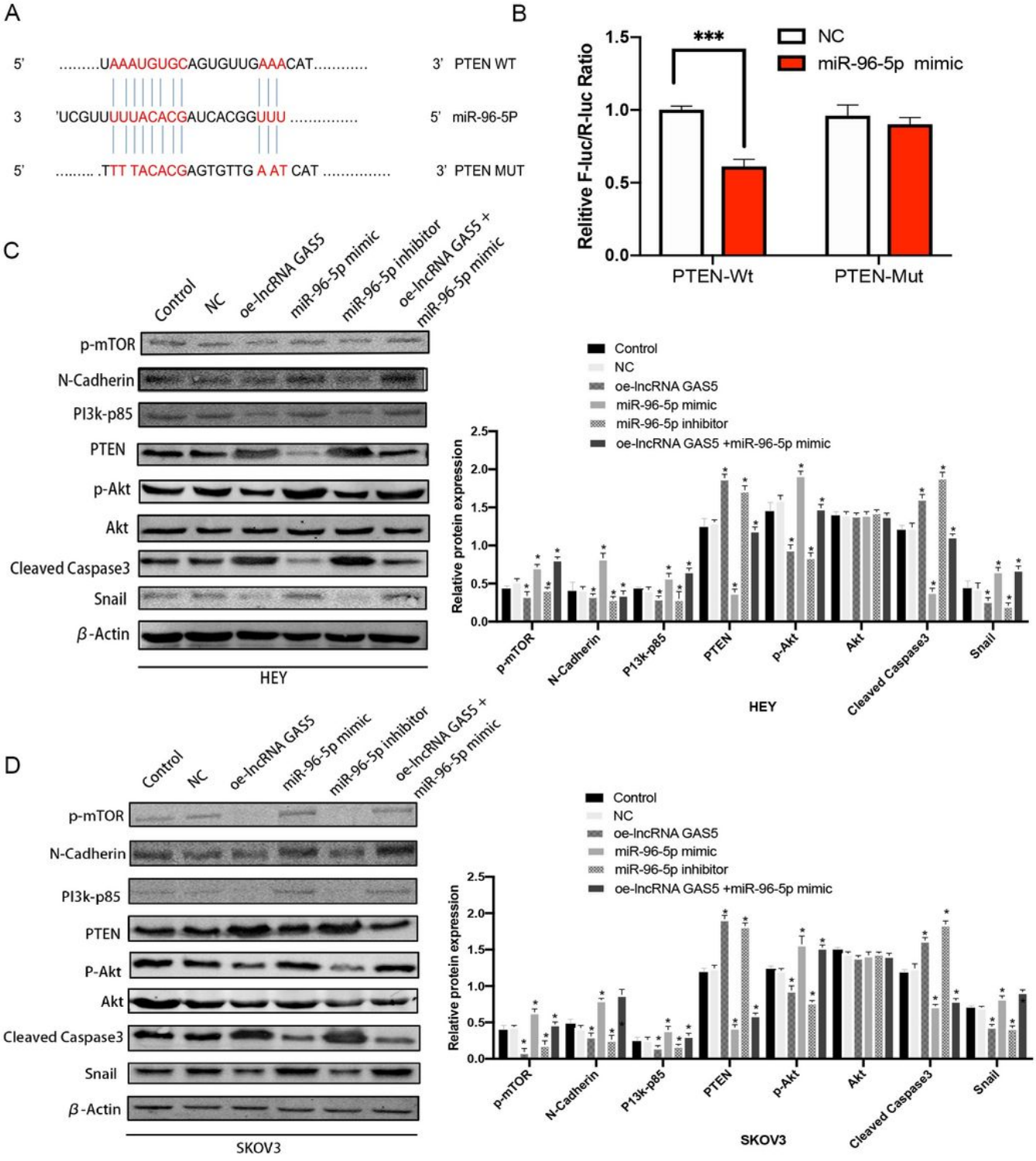

Figure 9

lncRNA GAS5 increases protein levels of PTEN and cleaved caspase-3 but decreases the phosphorylation of AKT, mTOR, N-cadherin and Snail. (A) The miR-96-5p binding site in the sequence of PTEN 3′ UTR. (B) Binding relationship between PTEN and miR-96-5p was detected by luciferase reporter assay with WT or Mut luciferase reporter plasmids of PTEN. (C) The protein bands of P-mTOR, N-cadherin, PI3K-p85, PTEN, AKT, p-AKT, cleaved caspase-3, Snail, and β-actin in HEY cells detected by western blot assay. (D) The protein bands of P-mTOR, N-cadherin, PI3K-p85, PTEN, AKT, P-AKT, cleaved caspase-3, Snail, and β-actin in SKOV3 cells detected by western blot. The data are presented as the mean ± SD and analyzed using one-way ANOVA. The experiment was independently repeated thrice. *, $P < 0.05$; **, $P < 0.01$; ***, $P < 0.001$.